Optimized Future Tractor Semi-trailer Combination

Shajan, Govind

Award date:
2021

Department of Mechanical Engineering
Automotive Technology
Dynamics & Control Research Group

Optimized Future Tractor Semi-trailer Combination

Master Thesis

G. Shajan
1348191

DC 2021.083

Supervisors

Dr. Ir. Igo Besselink, TU/e
Mr. Peter Joosten, Knapen Trailers B.V.

Prof. dr. Henk Nijmeijer, TU/e

Eindhoven, September 2021

Abstract

In the EU, road transport of goods is executed with tractor semitrailer combinations, whose dimensions and weights are prescribed in the EU Council Directive 96/53/EC. The maximum allowed weight of this vehicle combination is 40 tonnes. Regulation 96/53/EC, also states that the maximum allowed weight for a tractor semitrailer combination with 4 axles is 38 tonnes. With 2 minor modifications to the legislation, 1 axle can be eliminated. They are:

- Increase maximum axle load of the front axle of tractor from 7.5 ton to 8.5 ton
- Increase Gross Vehicle Weight for 4 axle from 38 ton to 40 ton.

By doing so, the semitrailer will be lighter but will require a steered rear axle which improves mobility during tight turns. This thesis investigates and quantifies the performance gains of a 2 axle semitrailer in comparison to the conventional 3 axle semitrailer used on roads today.

The performance comparison is done using Simscape Multibody, which is a 3D simulation environment that is a part of MATLAB Simulink. The model of the conventional tractor semitrailer has been adapted to match the specifications in terms of mass and dimensions of the trailer produced by Knapen Trailers and the proposed improved trailer with rear axle steering. Additional functionality has been added to these models to evaluate the Fuel Consumption and Tire Wear.

Testing of the safety performance via assessment using Performance Based Standards (PBS) has been conducted to investigate if the proposed vehicle combination is safe enough to be used in the most commonly encountered driving scenarios while operating in the EU.

Acknowledgements

Working on my Masters Thesis during COVID 19 has been a unique experience. I owe the successful completion of my thesis to the support and inspiration I received from many people, who have guided me in every step making sure that I dont falter.

In particular, I would like to thank my supervisor dr. ir. I.J.M. Besselink, for providing continuous guidance and encouragement. The comments that you have given during our discussions have guided me towards making the right decisions in many areas of this thesis.

Next, I would like to thank Mr. Peter Joosten of Knapen Trailers for his support and dedication towards ensuring that I had all the right tools at hand, to make this thesis the best it could be. Your words of advice and the questions you asked during our discussions have changed the way that I think when it comes to handling problems.

I would like to express my sincere gratitude to my Supervisor/Mentor Prof. dr. ir. H. Nijmeijer whose comments have motivated me to push myself to produce a better result. I admire your assessment of my work, and I feel grateful to have been mentored by you.

I offer my deepest gratitude to my parents and sibling, who have blessed me with their words of encouragement, which have given me the strength to persevere during these times. Had it not been for their support, I know I would not be where I am now. I would also like to thank my friends, who have provided me with ample love, stimulating discussions and much needed distractions to take my mind off of my research.

Contents

List of Figures

List of Tables

Nomenclature

Greek Letters and subscripts

α	side slip angle
α_t	equivalent side slip angle of axle group
σ	wear rate
ρ	density of air
ϕ_i	steering angle of inner wheel
ϕ_o	steering angle of outer wheel
δ_r	rear axle steering angle
δ_t	path following controller steering angle
ψ_{ps}	look ahead angle
ω_{ICE}	engine speed
τ_{ICE}	engine torque
γ	abrasion per unit of energy dissipation
$\ddot{\theta}$	yaw acceleration
$\dot{\theta}$	yaw rate

Latin Letters and subscripts

F_N	normal force
F_y	lateral force
F_x	longitudinal force
s	slip distance
V_w	worn volume
V_p	volume of plastic deformation zone
W_x	longitudinal work
$C_{F\alpha}$	cornering stiffness
w	width of tire
g	gravitational constant
m_n	sprung mass
h_n	COG height
a_{yn}	lateral acceleration at COG of sprung mass

$a_{y,rcu}$	lateral acceleration at COG of roll coupled unit
$\bar{A}_1$	amplitude ratio
D_1	yaw damping ratio
c_1	steering sensitivity
F_{aero}	aerodynamic drag force
A_f	frontal area of tractor
C_d	drag coefficient
$\dot{m}_f$	mass flow rate
C_{RR}	rolling resistance coefficient
F_{RR}	rolling resistance force
F_{RR-ISO}	rated rolling resistance force of tyre
Z_{RR_ISO}	rated normal load of tyre
P_{sy}	power loss in lateral direction of tyre
P_{sx}	power loss in longitudinal direction of tyre
K_w	scaling factor for tire wear
I_{zz}	moment of inertia about z axis
u	longitudinal velocity

Abbreviations

EEA	European environmental agency
EU	European Union
ARTSA	Australian Road Transport Suppliers Association
PBS	Performance Based Standards
CS	Command Steering
CVL	Commercial Vehicle Library
TS	Tail swing
DLTR	Dynamic Load Transfer Ratio
RA	Rearward Amplification
SRT	Static Rollover Threshold
RCU	Roll Coupled Unit
COG	Center of Gravity
BSFC	Brake Specific Fuel Consumption
RD	Regional Distribution
LH	Long Haul
G.V.W.	Gross Vehicle Weight
RAS	Rear Axle Steering
GPS	Global Positioning System

Chapter 1

Introduction

Road transport is the primary mode of transport for goods. Over the years, road transport has improved in quantity, speed and efficiency. Even now, it is a question if a better possibility exists. This is the basic question that this thesis attempts to understand and answer. Section 1.1 provides the necessary background information, to define the state of the art of heavy goods transport used in the EU and options to improve it. Section 1.2 presents the problem statement this thesis attempts to answer. Also, an overview of the important questions that need to be asked to justify the use of the proposed tractor semitrailer is provided here. Finally, Section 1.3 gives a brief outline of the contents of this thesis.

1.1 Background

Road transport has a distinct advantage over other modes of transport. Roads can be easily set up due to their lower cost of construction and maintenance when compared to railways and water ways. This allows remote locations to be made easily accessible. But the major drawback of road transport is that it still is a major contributing factor to Greenhouse gas emissions as can be seen from Figure 1.1.

Even though efforts to reduce CO_2 emissions have been increased in the manufacturing and raw material sectors of various industries over the last few decades, road transport sector still contributes heavily to green house gas emissions. In 2017, 27 % of total EU-28 greenhouse gas emissions came from the transport sector, with 22 % of international aviation and maritime emissions are excluded. CO_2 emissions from transport increased by 2.2 % from 2016. [1] Today, more than 70% of all goods in the EU are transported over the roads [1].

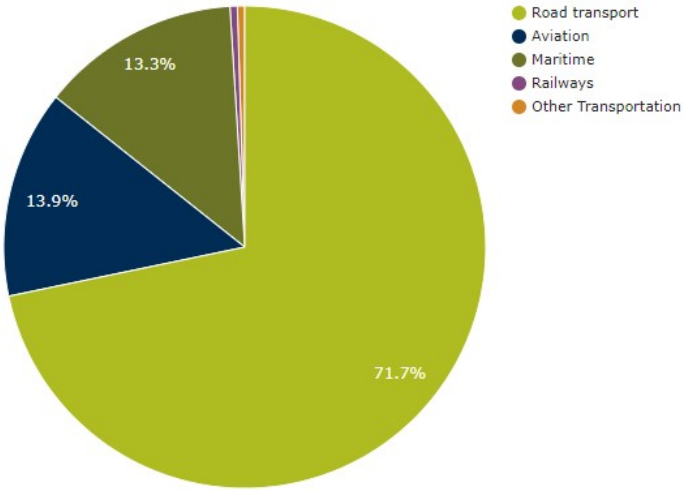

Figure 1.1: Contribution of road transport to greenhouse emissions [1]

The most common vehicle used to transport goods is the 5 axle tractor semitrailer as shown in Figure 1.2. The EU Council directive 96/53/EC governs its dimensions and weight [14]. The maximum allowed weight of the vehicle combination is 40 tonnes and that of a semitrailer with 3 axles is equal to 24 tonnes. The dimensions and weight of vehicle combinations are tightly regulated and have not changed significantly since 1996.

Figure 1.2: 5 axle Tractor Semitrailer

Even though the tractor semitrailer with 3 axles is being used as the industry standard, efforts need to be made to know whether this is the most optimal semitrailer setup. Removing an axle from the 3 axle semitrailer changes 2 things. The weight distribution of the trailer changes as each tyre now carries more load which means that the optimal wheelbase required to maintain the loading of 11.5 ton at the drive axle of the tractor (as specified in [14]) is different. Also, reconstructing the trailer chassis to accommodate 2 axles leads to weight savings (about 1000 kg) [15] which can be used to carry more payload provided the vehicles are allowed to share the same gross vehicle weight.

Regulation 96/53/EC, [14], states that the maximum allowed weight for a tractor semitrailer combination with 4 axles is 38 tonnes. With 2 minor modifications to the legislation, the 2 axle semitrailer can become a viable candidate to replace the 3 axle semitrailer for road transport in the EU. These are

- Increase maximum axle load of the front axle of tractor from 7.5 ton to 8.5 ton
- Increase Gross Vehicle Weight for 4 axle vehicle combinations from 38 ton to 40 ton.

When these modifications are made, the payload capacity of the 2 axle trailer is increased by 1000 kg making it similar in G.V.W. to the conventional tractor semitrailer, due to weight savings by eliminating one axle. However, a few alterations need to be made to the tractor. The optimal wheelbase from the 5^{th} wheel of the 2 axle semitrailer is calculated as 8.8 m. This is different from the optimal wheelbase of the 3 axle semitrailer at 7.75 m. Regulation 96/53/EC [14] also specifies that there needs to be a sweep radius of 2040 mm from the tractor 5^{th} wheel to the semitrailer. In order to achieve the same load distribution on the driven axle while adhering to the regulations of 96/53/EC , the wheelbase of the tractor is increased from 3.7 m to 4 m as shown in Figure 1.3.

Figure 1.3: 4 axle Tractor Semitrailer

To introduce this 4-axle combination in the EU, it must meet specific swept path requirements. The EU 360 circle is one such scenario used to test whether the newly proposed vehicles can deal with the road structures already in place in the EU. Here the vehicle combination is driving a steady state circle so that the outermost point of the tractor semitrailer tracks a circle of 12.5 m radius. The test criteria is that the inner radius of the innermost point of vehicle trajectory must track a circle with a radius of 5.3 m or greater.

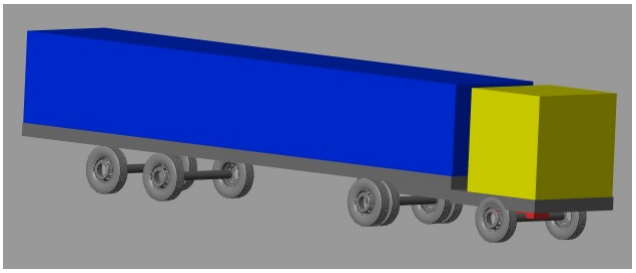

Figure 1.4: 4 axle Tractor Semitrailer in Simscape Multibody

The 4-axle vehicle combination without rear steering cannot meet this requirement. As shown in Figure 1.5, the 4 axle combination tracks an inner radius of 3.36 m, while the conventional 5-axle vehicle combination has an inner radius of 5.38 m. The simulations are made using the Simscape Multibody version of the TU/e Commercial Vehicle Library. Using this tool, one can build Tractor-Semitrailer combinations of a variety of geometries and study the performance of that vehicle combination. Figure 1.4 shows the 4 axle Tractor Semi-trailer visualized in Simscape Multibody. More details about the simulation environment of Simscape Multibody will be given in Chapter 3.

To allow this 4-axle vehicle combination to meet the EU requirements, a steered rear axle needs to be introduced which increases the inner radius to a value greater than 5.3 m. Inclusion of a steered rear semi-trailer axle gives the vehicle greater low-speed manoeuvrability. Also, lower lateral forces are generated at the trailer wheels. Quantifying the performance gains that can be gained by adapting this trailer will be a part of this thesis.

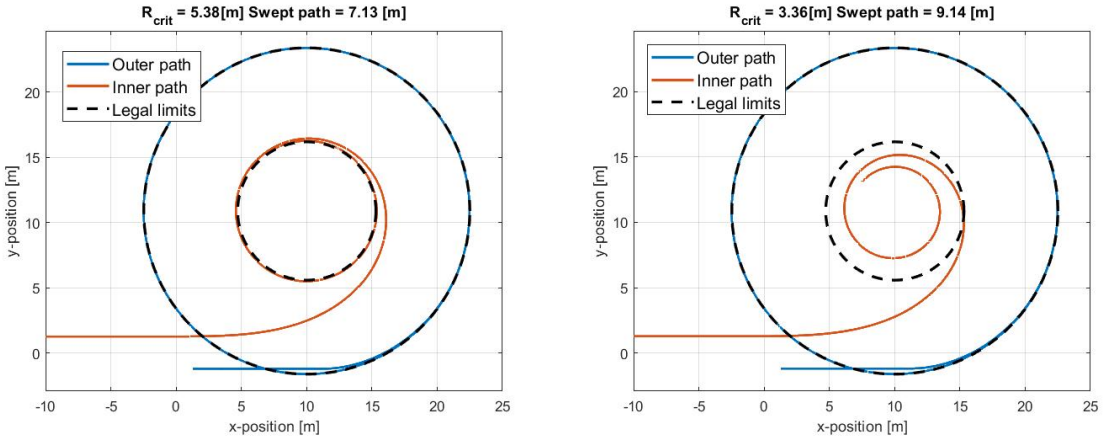

(a) 5 axle Tractor Semitrailer

(b) 4 axle Tractor Semitrailer without rear steering

Figure 1.5: Swept Path analysis - 5 axle vs 4 axle tractor semi-trailer without rear steering

1.2 Problem Description

The aim of this research is to find an optimal configuration for a tractor semi-trailer vehicle combination, that can be put into operation in the EU with minimal change to the rules in the EU Council Directive 96/53/EC [14].

Knapen Trailers claims that a 2 axle semitrailer with a steered rear axle will have significant advantages in terms of fuel Consumption, tire Wear and safety. To verify these claims and quantify the performance gains that can be obtained, tractor semitrailer models are created in the Simscape Multibody Environment.

The tractor semi-trailer model developed at the TU/e will be used as a starting point. This model represents a standard 5 axle tractor semitrailer that is commonly used to transport goods within the EU. The conventional tractor semitrailer model is adapted in dimensions and in mass to match the specifications of Knapen Trailers [15]. These models will be used to quantify the gains in performance in different areas. The baseline model does not have a power-train model to evaluate the fuel consumption. This functionality needed to be added to the model. It needs also to be known whether the 2 axle semitrailer having one less axle than the conventional trailer can lead to lower rolling resistance forces. To quantify tire wear, a formula will be proposed and implemented in the model that can evaluate the tire wear phenomenon that occurs due to the slip of the tires. Finally, the safety of the vehicle in its operation needs to be compared to the conventional tractor semi-trailer using Performance Based Standards.

To summarize, the main question that will be answered by this thesis is:

"Will the 2 axle semi-trailer with steered rear axle offer better performance compared to the 3 axle semitrailer to justify its operation in the EU?"

This question will be answered by quantifying the performance gains in terms of

- fuel consumption
- tire wear
- safety performance

The safety performance will be evaluated by simulating different manoeuvres defined in the PBS Standards of ARTSA (Australian Road Transport Suppliers Association). The performance will be evaluated using measures like swept path, tail swing, static rollover threshold, high speed off-tracking, rearward amplification and yaw damping. This will provide a clear picture on the applicability of the proposed tractor semitrailer combination for their use in the EU.

1.3 Outline

This thesis begins with an overview of the current state of the art in the areas of steering control and tire wear evaluation. A description of the PBS Standards used to evaluate the performance of proposed tractor semitrailer is also provided.

The next chapter discusses the simulation environment with which the results of this thesis are obtained. Here, the Simscape Multibody model of the tractor semitrailer is described, along with the various additions that were made to the original model, to arrive at the results in the following chapters. Chapter 4 will go over the corrections made to the rolling resistance in the Simscape Multibody model and the reduction in rolling resistance that can be expected from the proposed 4 axle tractor semitrailer. This chapter will also include the results of fuel consumption. Chapter 5 describes tire-wear performance. The modelling will be elucidated upon and a comparison of the difference in tire wear models will be presented. Chapter 6 will present a comparison of the proposed 4 axle tractor semitrailer with the conventional 5 axle tractor semitrailer in terms of performance measures by using the manoeuvres mentioned in the PBS Standards. Finally, Chapter 7 will present the conclusions drawn and the recommendations for future research.

Chapter 2

Literature Review

To propose a new type of trailer that can provide better performance compared to a conventional one, a clear understanding of the advancements that have been made in relevant research fields is necessary. This section of the report will discuss the current state of the art in the following areas.

1. Steering Control
2. Tire Wear
3. PBS Standards

2.1 Steering Control

Tractor semitrailers are among the most popular vehicles used for freight transport in the EU, due to their flexibility and transport efficiency. Despite the clear advantages given by such vehicles, they are not the most optimal solution for all transport scenarios. Particularly, they lack maneuverability to be driven on small roads or in urban areas with narrow streets. The poor maneuverability of tractor semitrailers is due to their length and lack of directional control. The trailer is steered only by the tractor steer axle in most cases, all other wheels are non-steered. The 5^{th} wheel provides an additional articulation angle compared to the rigid chassis of a truck. It affects high speed stability and safety of the vehicle. At high speeds phenomena like rearward amplification can occur, which may cause the trailer to swing excessively.

Another issue with tractor semitrailers is the tire wear during cornering. In order to lower the static axle loads per axle, today's trailers are fitted with multiple axle groups. When these axles are not steered, the tires tend to generate significant lateral forces when making tight corners wearing the tire heavily.

To address these issues, a number of passive steering systems have been proposed over the years. Here, the wheels on the trailer are steered using geometric relationships. Common steering systems include self-steering axles, command steered systems and pivotal bogie systems.

2.1.1 Self Steering systems

Self steering axles had initially been designed to be used as the second axle of a tandem axle group on trucks to improve off-tracking and reduce tire scrubbing during tight turns [2]. They had been adapted into trailers due to their influence in 2 areas. The ability of the self steering axle to improve the cornering characteristics during steady state turns and its ability to resist unbalanced longitudinal forces (uneven braking).

The tyres of the self steered axle are aligned in the direction of travel during low speed turns. The spring constant of the springs that hold the wheels in position is only high enough to correct slight variations in steering angle (when encountering uneven longitudinal forces) and do not provide any cornering stiffness to the axle. The effective wheelbase is thus shortened since the self steering axle generates little lateral force when cornering. This improves low speed manoeuvrability at the expense of high speed stability.

2.1.2 Pivotal Bogie systems

Pivotal bogie systems consist of a roll-coupled bogie replacing the fixed axle group of a regular semi-trailer. The roll-coupling allows yaw degree of freedom between the axle group and the trailer chassis. The bogie shown in Figure 2.1 consists of a fixed front axle and two steered rear axles, which are steered with respect to the angle between the bogie and the trailer chassis. Bogie designs consisting of 2 axles with front axle steering are also commonly used in the EU. As the trailer is steered, the steering angle of the steered wheels are increased proportionally, bringing the bogie back in line with the trailer chassis, while greatly reducing the critical radius of cornering. There is a great shortening of the effective wheelbase when turning as the fixed front axle of the bogie always orients itself away from the trailer chassis, making the perpendicular drawn from the effective axle intersect with the perpendicular from the drive axle of the tractor at a point ahead of the bogie. This brings the instant center of turning closer to the trailer.

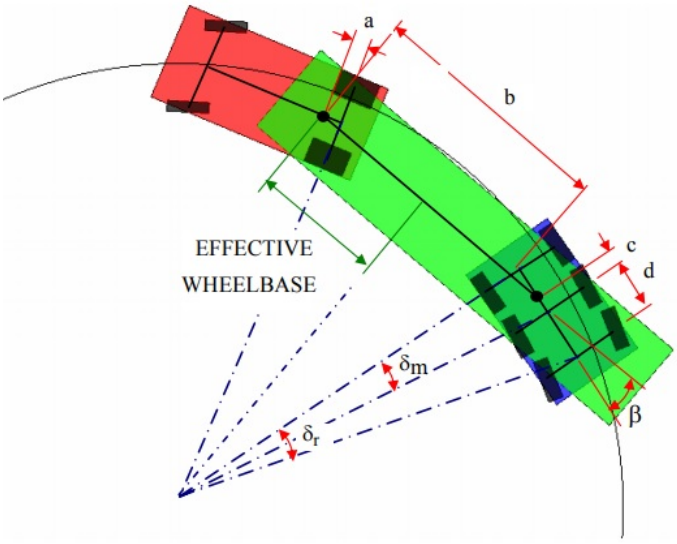

Figure 2.1: Pivotal Bogie System at low speed [2]

2.1.3 Command Steered systems

A command steered trailer usually has the rear most axle(s) of the semitrailer steered, while the front axle is non-steered. The steered axles are forced to steer in relation to the articulation angle between the tractor and the semitrailer. Usually the articulation angle is measured using an electronic sensor or mechanically using a special ball bearing attached to the trailer side of the 5^{th} wheel.

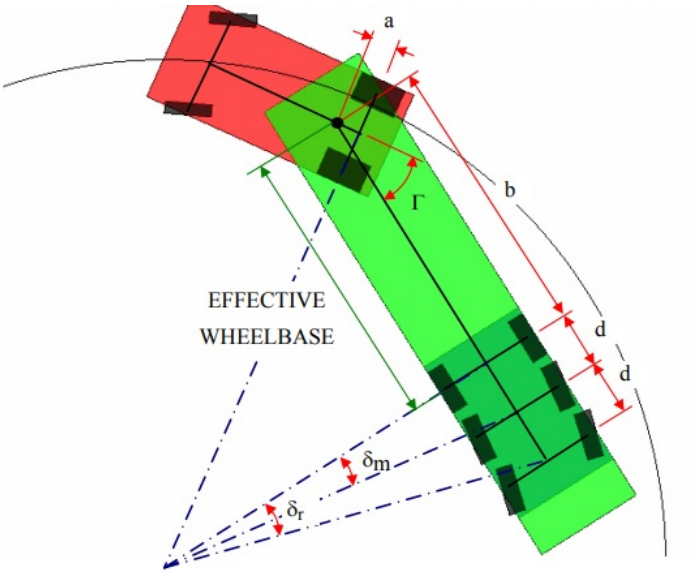

Figure 2.2: Command Steering System at low speed [2]

Among these approaches, the command steered approach is chosen to realize rear axle steering in this thesis, due to its simplicity and ease of implementation in real life. The equations that control the steering input can be obtained by considering the tractor semitrailer during a low speed turn. To ensure that there is negligible side slip angle, the rear wheel is steered so that the normal to the steered wheels passes through the instant center of rotation as that of the first non-steered axle. Since negligible lateral forces are generated by wheels of all axles, the wheelbase of the semitrailer is reduced significantly compared to its non-steered counterpart. This positively affects the low speed manoeuvrability.

Command steered systems have been studied extensively by Sankar et al [16]. Another interesting work is that of Rangavajhula and Tsao [17] where a form of active command steering control had been investigated.

It is to be noted that these systems improve the low speed maneuverability, but are known to have a negative effect on the high speed stability. They usually tend to cause high rearward amplification. This thesis aims to investigate the impact of such steering on high speed stability. To overcome this issue, many newer active steering control methods have been suggested like the CT-AT controller from Jujnovich and Cebon [2] and the lead point follow point approach from Wouters et al [18] and [19]. But these are not easy to implement within the time-frame of this project and the choice to implement a command steering mechanism

had been made. Another approach is to lock the steered axles when the trailer is moving above a velocity threshold. The effectiveness of this method compared to keeping command steering active at high speeds is also investigated.

2.2 Tire Wear

Tires are arguably among the most important parts of a road vehicle as they are the only point of contact of the vehicle to the road it operates on. Understanding the behaviour of tires is a field of active research and will grow in importance in the near future as vehicles become more energy efficient and are capable of transporting more goods. Tyres of the modern day are much more capable than what they used to be. Back in 1839 American Inventor and entrepreneur Charles Goodyear discovered the vulcanization process. With this process, natural rubber had been made into more durable materials with the addition of sulphur and gave it superior mechanical properties, elasticity and weather resistance. It also made the tire pliable, making vulcanized rubber the perfect material for tires. Earlier rubber tires had been solid, which later became pneumatic as they had better shock absorption properties, reduced vibration and increased traction in vehicles. Soon in 1920, Bias Ply tires were being made in Germany using synthetic rubber with an inflated tube and casing, which greatly improved traction and were used for over 50 years. Then, after World War 2, Michelin introduced radial tires which outperformed bias-ply tires due to their superior handling and fuel economy. Radial tires dominate the market today with almost 100 percent market share.

With all the advancements made in the development of tires over the last century, one major problem still remains and continues to claim the lives of tires all over the world: Tire Wear.

Initial developments of models that predict tire wear had been analytical models based on normal pressure distribution and sliding distance covered by the tread element. Among the models that are available publicly, these are the most discussed.

2.2.1 Archard's Wear Law

Also known as the Reye-Archard-Khrushchov law, this wear law was conceived by the contributions of Theodor Reye, John Frederic Archard and Michael Michailovich Khrushchov. This law was used during a time when metal wheels had been used considerably (railway bogeys) and is most appropriate for the wear of metal disks. However, they had been experimentally found to be sufficient in describing the wear behaviour of modern day tires, as shown in [20]. The wear law can be stated as:

$$V = \frac{F_N \cdot s}{H} \cdot k \tag{2.1}$$

where V is the volume of worn material, in mm^3, F_N is the normal force [N], s is the slip distance [mm], H is the material hardness [N/mm^2], and k is a dimensionless wear coefficient.

The wear coefficient k is defined in literature [21] as the wear volume fraction at the plastic deformation zone.

$$k = \frac{V_w}{V_p} \tag{2.2}$$

where V_w is the worn volume and V_p is the volume at the plastic deformation zone. It varies from a value of 10^-7 to 10^-3 for metallic materials [22]. For rubber, an appropriate value is not known.

Then using Reyes Hypothesis, which states that "the volume of material lost due to adhesive wear effects is proportional to the work performed by the friction forces" [23], we get

$$V = \frac{W_x + W_y}{H} \cdot k \tag{2.3}$$

where

$$W_x = F_x \cdot s_x \tag{2.4}$$

$$W_y = F_y \cdot s_y \tag{2.5}$$

where W_x and W_y are the longitudinal and lateral work [N.mm] and s_x and s_y are the longitudinal and lateral slip distance of the contact patch [mm].

2.2.2 Schallamach's Wear Law

The Schallamach's wear law is defined in [24] as

$$Q = \gamma \cdot s \cdot F_N \tag{2.6}$$

where Q is the abrasive wear quantity, γ is the abrasion per unit of energy dissipation, s is the sliding distance and F_N is the normal force.

The unit of the wear quantity, however, are not mentioned by Schallamach [24].

These models can predict wear that occurs in tires to an acceptable accuracy, but they do not combine the dependence of load and slip. Many more simple analytical models for tire wear prediction exist, but they are only applicable under a large number of assumptions, for example small slip angles, fixed tyre abradability characteristics, linear cornering stiffness, measurable contact stiffness, etc. This limits the applicability of these models to tires in real life.

When operating on the road, tyre wear occurs across 2 regimes.

- when the vehicle is accelerating or decelerating in a straight line due to longitudinal forces
- when a vehicle is cornering due to lateral friction forces

Even within these regimes of operation, tire wear occurs due to many factors such as the dynamics of the tire and the vehicle, structure of the tire, the tyre road interaction, tire and ambient temperature and mechanical properties (eg. hardness, abrasion characteristics, damping) [25], [26]. Relying on completely analytical tire wear models to predict tire wear will not give reliable results.

Li et al. [3] did a parameter sensitivity study to compare the magnitudes with which key parameters that affect tire wear do so. As can be seen from Figure 2.3, among the many parameters that tire wear is dependent upon, we see that the influence of side slip angle is the most prominent.

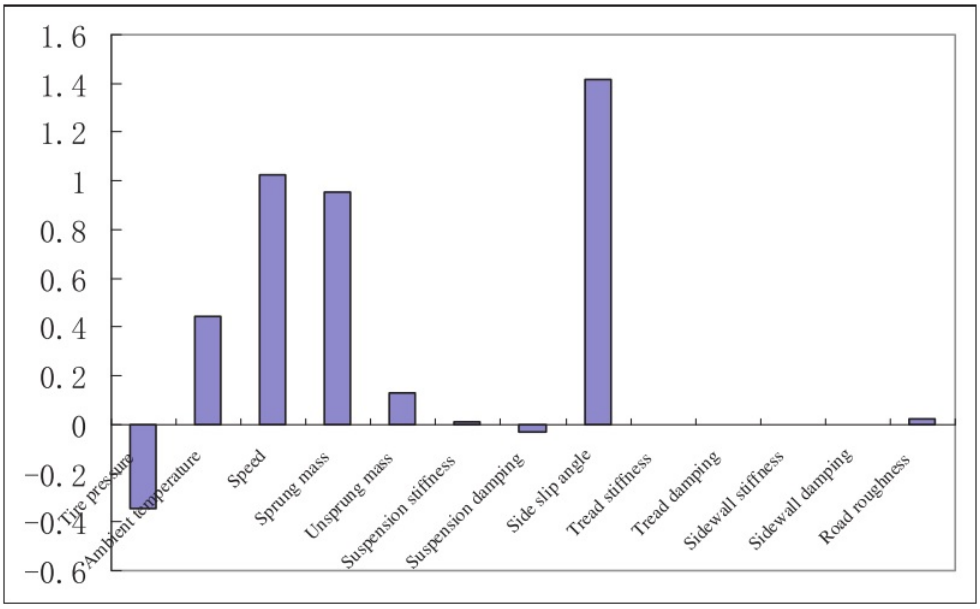

Figure 2.3: Comparative histogram of factors affecting Tire Wear [3]

Also for tyres used in heavy goods vehicles, like a tractor semitrailer, the lateral abrasive wear is the principal source of in-service wear, because large braking and accelerating forces for drive axles causing longitudinal slip are not frequent [5]. Thus, to gain accurate information of the savings that can be obtained by the proposed tractor semitrailer combination, it is important to include slip angle in the assessment of tire wear, while keeping the other parameters constant, as to get a rough estimate of tire wear during certain manoeuvres.

A brief background on the generation of slip angles in a non-steered trailing unit is provided next. A vehicle is able to turn due to the generation of side slip forces acting perpendicular to the plane of symmetry of the tyre. The magnitude of slip force is calculated using

$$F_y = C_{F\alpha} \cdot \alpha \tag{2.7}$$

where α is the slip angle, which is the angle between the direction of travel of the wheel and the plane of symmetry of the tyre [27].

Whenever a vehicle having a non-steered axle group negotiates a turn of small radius, substantial slip angles are generated at certain tires. Scrubbing forces of considerable magnitude are generated during such a turn and severe abrasive tyre wear occurs on the tires where the slip angles are the highest. The slip angles for a non-steered axle group increases proportional to the distance from the 'virtual wheel axle' or 'effective axle'. As can be seen from Figure 2.4, the slip angle of a tyre α is the angle between the velocity vector the tyre wants to move towards and the instantaneous direction of travel of the tyre. Since the effective axle rep-

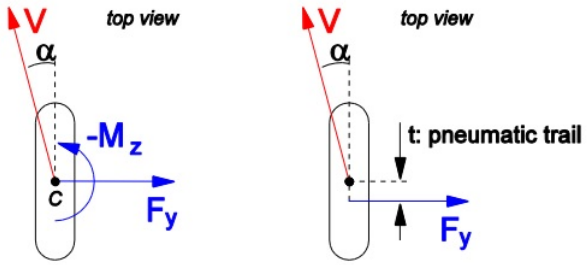

Figure 2.4: Lateral force generated by Side slip [4]

resents the line which meets the instant center of cornering, it represents the steering point of the trailer, where the direction of the velocity vector matches the instantaneous direction of travel. So at the effective axle, the slip angle is almost always zero. When the distance from the effective axle increases, the distance of the perpendicular drawn from that axle to the instant center of cornering increases, which causes further deviation between the velocity vector and the tyre's plane of symmetry. This increases the slip angle, which results in the scrubbing of tyres.

2.2.3 Empirical Estimation of Heavy Goods Tyre Wear

D. Cebon and J. Lepine [5] developed a novel technique for measuring tire wear using a semitrailer equipped with an active steering system. With the trailer steering system, one can recreate wear at different slip angles under controlled conditions in a controlled environment such as an asphalt test track. The active steering system allows independent steering of each trailer axle of the tri-axle setup.

Hence, the trailer was made to move in a straight line by giving the 2^{nd} and 3^{rd} rear axle slip angles of $+\alpha$ and $-\alpha$ respectively. Since the slip forces generated at these axles are equal and opposite, they negate each other and the trailer moves in a straight line. This allows the first axle of the 3 axle trailer to be steered to achieve the necessary slip angle, as shown in figure 2.5.

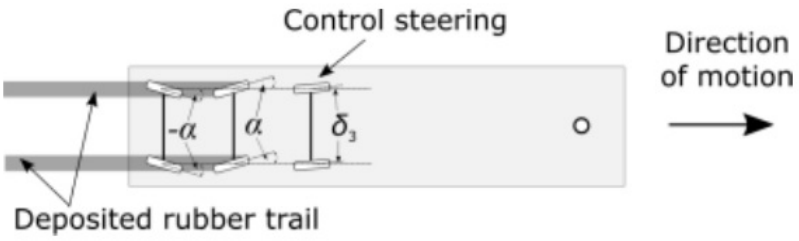

Figure 2.5: Experimental Setup in [5]

The slip angle had been increased as a step input from 0° to 14°, with a normal load of 100 kN acting on each axle. Tyre wear had been quantified by measuring the amount of rubber deposited on the road surface using a vacuum cleaner and a wooden jig of a specific surface area. The measurements show that the wear rate per unit surface area is represented

using a quadratic function:

$$\sigma(\alpha) = K\alpha^2 \tag{2.8}$$

with $K = 145$ g/m^2, and α measured in radians.

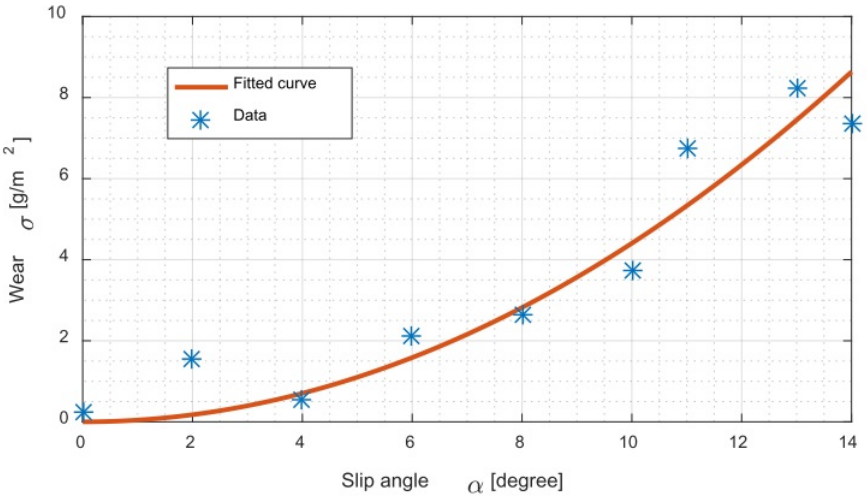

Figure 2.6: Wear as function of Side Slip Angle [5]

Now the tire wear can be calculated as a function of slip angle, $\alpha(s)$, for each tyre along a given path. The mass of rubber worn from each tyre is calculated by integrating,

$$\Delta M = w \int_{s=0}^{s_{end}} [\sigma(\alpha(s))] ds \tag{2.9}$$

where w is the width of the tire and s is the distance travelled by the tire.

2.3 PBS Standards

Performance Based Standards are used in countries like New Zealand, Australia and Canada to categorize a new HCV based on its performance for standardized testing conditions. If the HCV shows a certain level of performance, it is eligible for operation within a certain road class. Although this type of testing is not done in Europe, where vehicles are mainly classified according to their dimensions and weights, it is useful to compare the level of performance that can be obtained using these standardized testing procedures.

The focus of the thesis is on evaluating the maneuverability and stability that can be obtained from the proposed configuration of the 4 axle tractor semitrailer with a command steered rear axle in comparison to the common 5 axle tractor semi-trailer. Testing will be done using the following manoeuvres:

- EU 360° turn
- Static Rollover

- Single Sine Steering
- Pulse Steer

The performance measures are used to evaluate 3 configurations of vehicles:

- The conventional tractor and semitrailer with 3 axles
- The tractor and semitrailer with 2 axles where the rear axle has command steering
- The tractor and semitrailer with 2 axles with no steering input to the trailer axles

Testing is done in the fully loaded condition. It is to be noted that these performance measures can be obtained either via real life testing or software simulations. This thesis utilizes the Simscape Multibody version of the TU/e CVL to evaluate the tractor semitrailer combinations. More information about the simulation environment and the model is given in the subsequent chapter.

2.3.1 EU 360° turn

The first manoeuvre used to test the tractor semitrailer combinations is the EU 360° turn. The tractor is steered such that the outside wheel of the front axle follows a circular path with constant radius. From this, the performance measures of Swept Path and Tail Swing can be measured. The European International Traffic Regulations states that: "Any motor vehicle or vehicle combination which is in motion must be able to turn within a swept circle having an outer radius of 12.50 m and an inner radius of 5.30 m." So, the minimum swept path requirement is 7.20 m.

Swept Path

When the tractor semitrailer combination is making a circular turn, the trailing unit always tracks a path that is towards the inside of the turn. This means more space is taken when turning, which could lead to a collision with roadside objects or infrastructure. The Swept Path can be defined as the radial distance between the outermost trajectory of the cabin and the innermost point of the last semitrailer. To calculate the swept path, the trajectory of the outer edge of the cabin and the innermost edge is tracked and after the simulation the swept path is calculated.

Tail Swing

Tail Swing is the maximum lateral displacement towards the outside of the turn, measured from the rearmost point of the vehicle. It is the lateral displacement between the trajectory of the outermost point of the semi-trailer and the entry path tangent. The main factor that affects tail swing is the rear overhang, which can be defined as the distance from the effective axle to the end of the trailer body. The effective axle is the imaginary axle on the trailer body which always intersects the instant center of a turn without any steering at the tires. It is the axle that represents the action of an axle group as a whole. In general, the greater the tail swing value, more space is required to accommodate the vehicle during a turn. A lower tail swing value means that less space is required on the road to accommodate the vehicle.

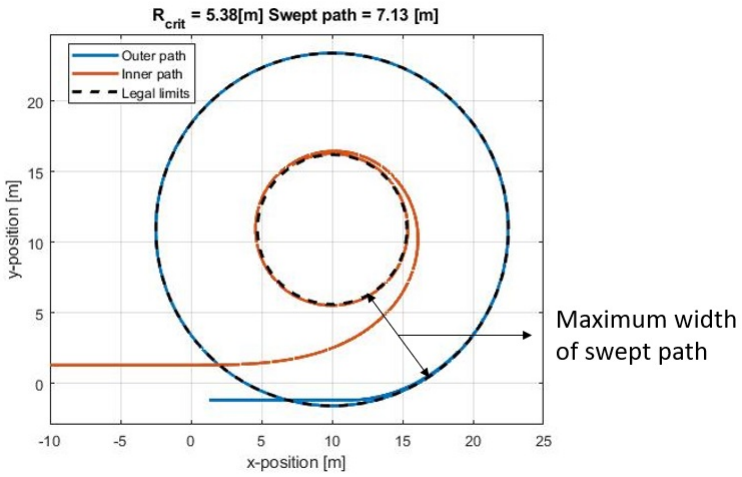

Figure 2.7: Swept Path of the conventional Tractor Semitrailer

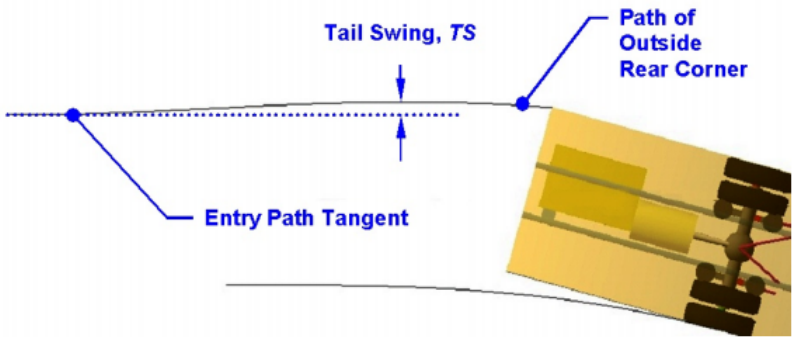

Figure 2.8: Tail Swing during EU 360° turn [6]

2.3.2 Static Rollover Manoeuvre

When a vehicle is cornering, lateral accelerations are induced on the vehicle body. These lateral accelerations cause load transfer, which shifts the vertical forces from the inside to the outside tires. The tractor and semitrailer are coupled using a 5th wheel coupling, which causes the roll-moment to be transferred from the trailer to the tractor. This improves the roll-stability of the vehicle, but as the lateral acceleration experienced increases beyond a certain threshold, the vehicle will roll over. The Static Rollover Threshold is a measure of the level of lateral acceleration that the vehicle can handle, beyond which rollover occurs. This performance measure gauges the likelihood of rollover to occur when cornering at high lateral accelerations.

The manoeuvre to measure Static Rollover Threshold can be summarized as follows. The vehicle must be steered such that the center of the steer axle follows a circular path of radius 100 m. The initial velocity of the vehicle is 50 km/h and the vehicle is gradually accelerated with a constant rate of 0.139 m/s^2 till rollover occurs. Rollover instability is achieved when the vertical forces on all the tires along one side of the vehicle are equal to zero, excluding the tires on the lightly loaded side of a steer axle with soft springs [18]. When the tires on one

side lose contact with the road, they can no longer generate the lateral forces. Now, rollover instability is achieved.

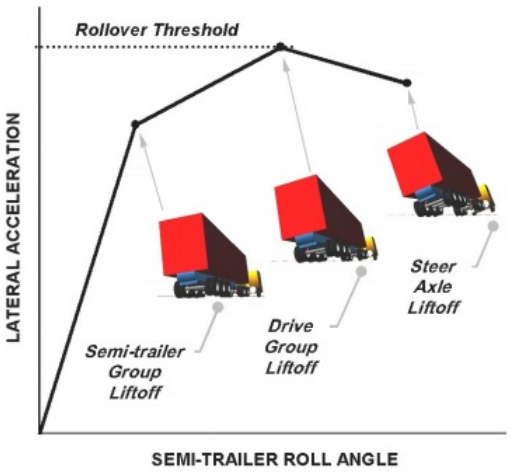

Figure 2.9: Lateral acceleration vs roll-angle of tractor semi-trailer [6]

The point in time when wheel liftoff is achieved can be evaluated using the Dynamic Load Transfer Ratio (DLTR). It can be seen from Figure 2.9 that the point in time that is defined as wheel liftoff is that time when the drive axle of the tractor semi-trailer lifts off the ground. It is at this point in time that the highest lateral acceleration is observed. Dynamic Load Transfer Ratio is a measure of the distribution of vertical tyre force between the left and right side of the vehicle at a given time instance. It is defined as:

$$R_{DLTR} = \frac{-(\Sigma_{n_{inner}=1}^{N_{inner}} F_{z_{n_{inner}}}) + (\Sigma_{n_{outer}=1}^{N_{outer}} F_{z_{n_{outer}}})}{\Sigma_{n_{inner}=1}^{N_{inner}} F_{z_{n_{inner}}} + \Sigma_{n_{outer}=1}^{N_{outer}} F_{z_{n_{outer}}}} \tag{2.10}$$

In this equation, N_{inner} and N_{outer} represents the total number of wheels on the inside and outside of a turn respectively for a vehicle unit and $F_{z_{n_{inner}}}$ and $F_{z_{n_{outer}}}$ represents the vertical tire force of the n_{inner} and n_{outer} wheel. The load transfer ratio is calculated as the difference in vertical tire force between the tires on the left side of the vehicle and the right side of the vehicle divided by the total vertical force. When the vehicle stands still, the DLTR is 0 and when the vehicle is close to rolling over, the DLTR becomes 1.

The lateral acceleration divided by the gravitational constant at which rollover instability occurs is defined as the Static Rollover Threshold. When DLTR is equal to 1, rollover instability is said to have occurred. The lateral acceleration is determined for a roll-coupled unit. A roll-coupled unit can be defined as an entire set of units that are coupled only with 5^{th} wheel couplings. The tractor semitrailer can be considered as a roll coupled unit, and the resultant lateral acceleration $a_{y,rcu}$ is calculated according to the following formula.

$$a_{y,rcu} = \frac{\Sigma_{n=1}^{N} m_n h_n a_{yn}}{\Sigma_{n=1}^{N} m_n h_n} \tag{2.11}$$

where m_n represents the sprung mass of a vehicle unit, h_n represents the COG height and a_{yn} represents the lateral acceleration at the COG of the sprung mass. The subscript n represents the nth vehicle in the rollcoupled unit and the total number of rollcoupled units are represented by N. [6]

So after the Static Rollover Manoeuvre is simulated, the first instance of time at which the DLTR is equal to 1 is determined, and the resultant lateral acceleration $a_{y,rcu}$ is calculated for the tractor semitrailer combination.

2.3.3 Single Sine Steer Input

The lateral dynamic stability of a tractor semitrailer can be evaluated using the single sine lane change manoeuvre. This scenario represents an obstacle avoidance/high speed lane change manoeuvre at high velocity. The Single Sine steer input (Figure 2.10) is defined by ISO 14791:2000(E) [7]. The vehicle should be moving at 88 km/h and the steer input should generate a lateral acceleration of 0.15 g at the steer axle, while having a frequency of 0.4 Hz. The amplitude of the steer input is different for each vehicle combination to meet the 0.15 g requirement.

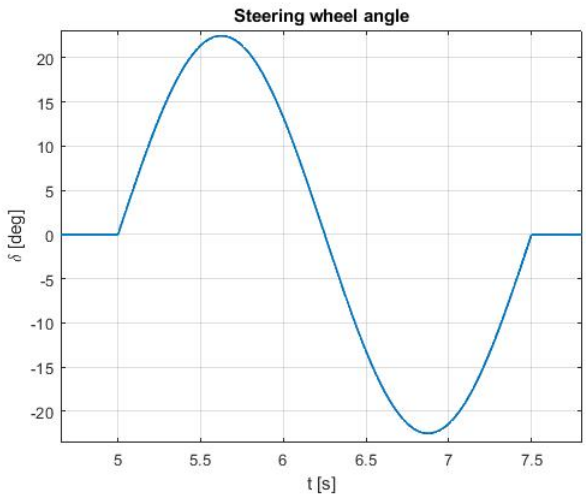

Figure 2.10: Single Sine Steer Input

The manoeuvre is used to calculate two performance measures: high speed off-tracking and rearward amplification.

High Speed Off-tracking

This performance measure is used to "assess the sway of the rearmost semi-trailer during a single sine manoeuvre at high velocity". At high speeds, when the tractor makes a lane change, the trajectory of the trailer has a larger amplitude than the path tracked by the tractor. The off-tracking performance or "overshoot" is defined as the maximum lateral displacement between the path followed by the center of the rearmost axle of the last semitrailer of the vehicle unit and the exit tangent of the tractor's steer axle. The higher the overshoot,

higher the chance of collision with infrastructure or other vehicles on the road.

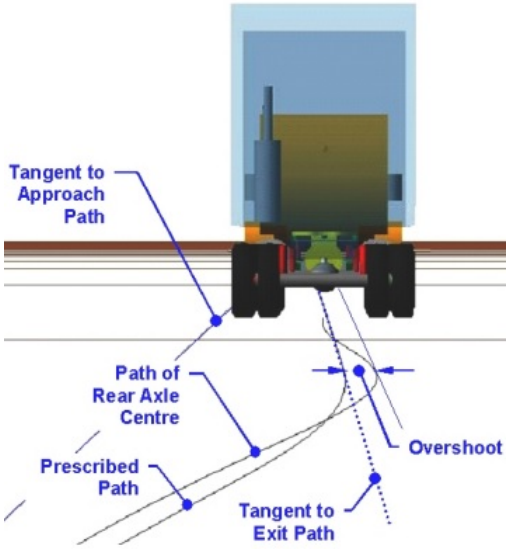

Figure 2.11: High Speed Off-tracking [6]

Rearward Amplification

The rearward amplification is used to assess the risk of rollover during a high speed lane change manoeuvre. There is an amplification of lateral acceleration from the tractor steer axle to the last axle of the semitrailer.

Rearward Amplification is defined as the ratio of the maximum absolute lateral acceleration at the center of gravity of the last roll-coupled vehicle unit to the lateral acceleration of the steer axle. Rearward Amplification reduces with fewer articulation points, roll-coupling, larger trailer wheelbases, tyres with higher cornering stiffness and shorter distance between the couplings and COG of the hauling unit [28].

The rearward amplification of a tractor semitrailer can be calculated with:

$$R_{RA} = \frac{max(|a_{y,rcu}|)}{max(|a_{y,sa}|)} \tag{2.12}$$

$a_{y,rcu}$ is the resulting lateral acceleration of the last roll-coupled unit, $a_{y,sa}$ represents the lateral acceleration of the steer axle of the tractor. Large values of rearward amplification are undesirable, as this indicates a greater risk of rollover during obstacle avoidance.

2.3.4 Pulse Steer Input

When an articulated vehicle, such as a tractor semi-trailer, changes direction at high speed, lateral forces are introduced at the 5^{th} wheel of the trailer. This generates yaw moment at the trailer, introducing slip angles and slip forces. These slip forces are large enough at high

speeds to cause oscillations in the trailer trajectory for a single pulse steer input. Thus, oscillatory behavior can be seen with the yaw-rate, which is measured as Yaw Damping. This criterion assesses the safety risk by requiring acceptable attenuation at any sway oscillations.

Yaw Damping

ISO 14791:2000(E) [7] states that the yaw damping is measured using a Pulse Steer Input. The ISO 14791:2000(E) Steering Impulse should have an amplitude high enough to produce a lateral acceleration of the first unit of 2 m/s^2, but it may be decreased for the purpose of limiting the response of the last unit to no more than 75 percent of the estimated rollover limit and no more than 75 percent of any tyre friction limit. The time period of the steering impulse should be less than or equal to 0.6 s and the time period of the corrections should not exceed 1.5 s.

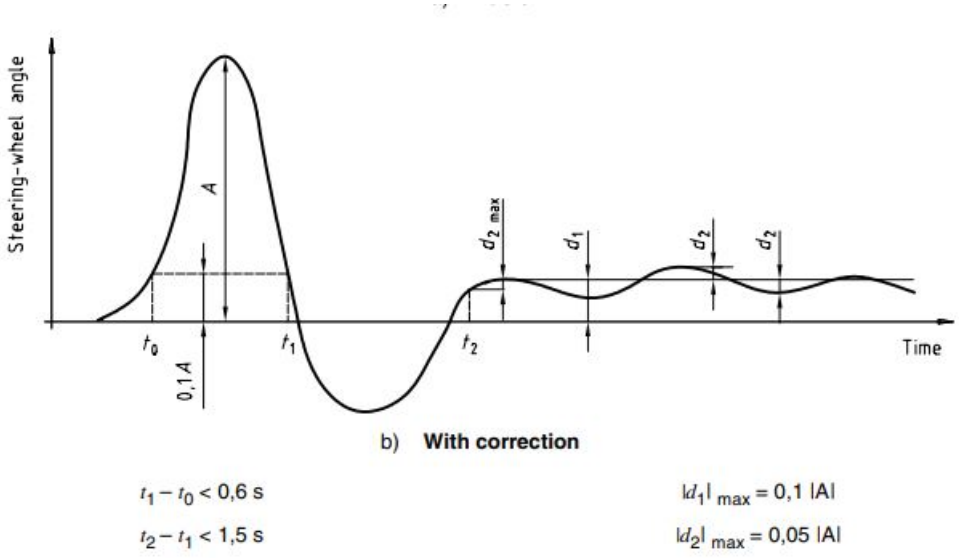

Figure 2.12: Pulse steer input [7]

It is to be noted that since the test is also to be conducted in practice, only time periods are mentioned in the standard. The Gaussian membership function is used to generate a steer input according to the specification mentioned in Figure 2.12. This function computes fuzzy membership values using the gaussian membership function:

$$f(x;\sigma,c) = e^{\frac{-(x-c)^2}{2\sigma^2}} \tag{2.13}$$

where σ is the standard deviation and c is the mean. More about the gaussian membership function can be seen in [29].

The yaw damping coefficient can be determined with the time history of either the articulation angle, articulation angle velocity or the yaw rate of the last vehicle unit. Figure 2.13 shows the typical trend of yaw rate of an articulated vehicle during a pulse steer input. To

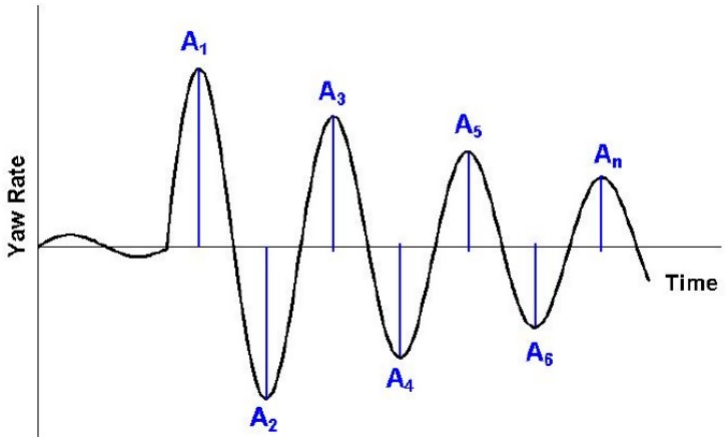

Figure 2.13: Yaw rate of an articulated vehicle during pulse steer input [6]

calculate the yaw damping coefficient of the chosen signal, the yaw amplitude ratio A is first calculated. As per the number of amplitudes available, yaw rate amplitude ratio is calculated as the ratio between consecutive peak amplitudes or consecutive amplitudes of the same sign.

$$\bar{A_1} = \frac{1}{n-2}(\frac{A_1}{A_3} + \frac{A_2}{A_4}.... + \frac{A_{n-2}}{A_n}) \tag{2.14}$$

or

$$\bar{A_2} = \frac{1}{n-1}(\frac{A_1}{A_2} + \frac{A_2}{A_3}.... + \frac{A_{n-1}}{A_n}) \tag{2.15}$$

The number of peaks n is equal to the number of peaks until the peak amplitude of the oscillation reaches a value of 5 percent of the maximum value. The oscillations are said to have died out after this point in time. $\bar{A_1}$ is calculated using (2.14) when the value of n is greater than or equal to 6. When n is lesser than 6, amplitude ratio $\bar{A_2}$ is calculated using (2.15).

Depending on the number of amplitude peaks n, the damping ratio can be calculated with:

$$D_1 = \frac{ln(\bar{A_1})}{\sqrt{(2\pi)^2 + [ln(\bar{A_1})]^2}} \tag{2.16}$$

or

$$D_2 = \frac{ln(\bar{A_2})}{\sqrt{(\pi)^2 + [ln(\bar{A_2})]^2}} \tag{2.17}$$

Higher the yaw damping ratio, more effectively the yaw oscillations are damped. Damping ratio of 1 means that the system is critically damped, while a damping ratio of 0 means that the yaw oscillations are not damped at all. Note that a lower number of articulations and axle groups positively impact yaw damping ratio. Yaw damping is also improved by increasing the roll center height and better suspension systems.

2.4 Summary

This chapter presents the prerequisite knowledge that the reader should know to gain an in-depth understanding of the work done in this thesis. The section on steering control presents the various trailer steering systems that are used in practice today and their pros and cons. The reason why command steering has been chosen for analysis is elaborated upon. The section on tire wear presents the relevant works that have been reviewed which lead to the selection of the method of tire wear evaluation used in this thesis. The section on PBS Standards describes both the manoeuvres followed and the performance measures used in the classification of safety performance of the compared tractor semi-trailers presented in Chapter 6.

Chapter 3

Simscape Multibody and Tractor Semitrailer model

The modelling of the tractor semitrailer has been done in the Simscape Multibody environment. Simscape Multibody provides a multibody simulation environment for 3D mechanical systems, such as robots, vehicles, construction equipment [30]. The equations of motion are formulated and solved for the mechanical system. Control systems can be tested and system level performance can be assessed to gain an idea of the level of performance that can be achieved in the real world. The modelling is done by representing each component of the object that is modeled using bodies of a specific mass and inertia and specifying the relation of each component to another using a system of joints. Force elements can be specified if a certain body experiences a force in a particular direction and measurements of the necessary variables that represent the motion of the body can be made using sensors.

3.1 Simscape Multibody

Simscape Multibody defines the position of each component of the model using a system of frames [31]. When defining a Simscape Multibody model, a few basic components are required. They are the world Frame, the solver configuration and the mechanism configuration. The World Frame represents the global origin of the model. The World Frame is the base frame to which all other frames are follower frames. The components of the system are defined using body blocks, where the geometry, mass and inertial properties can be specified [32]. Usually, the geometric center of each body block holds the location of the body's local reference frame. The position of a frame is always translated with respect to another frame using a block known as the rigid transform. The solver configuration is used to specify the type of solver that should be used to solve the differential equations formed by the model. Within the mechanism configuration, the gravitational acceleration field can be defined. Figure 3.1 shows the components that are described.

The visualization of the model is realized through the mechanics explorer, which is integrated into Simscape Multibody. This allows the user to see how the components of the model interact with one another when the simulation is run; this is shown in Figure 3.2.

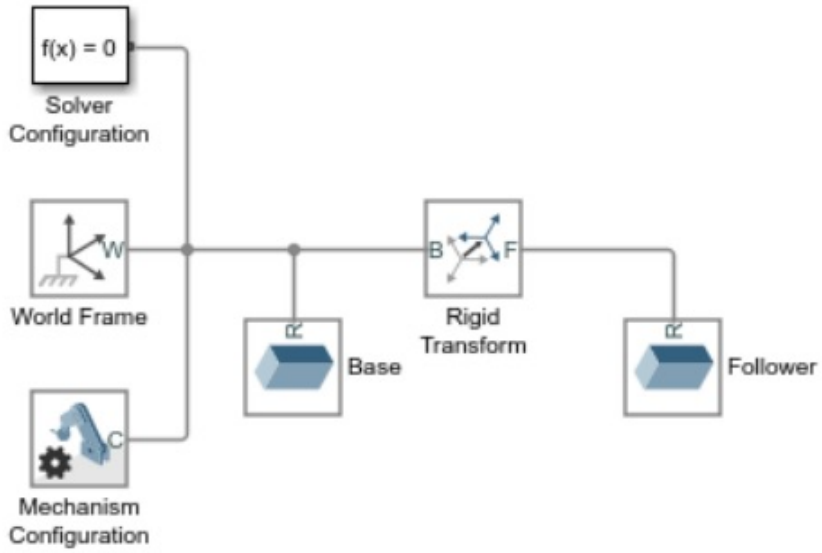

Figure 3.1: Key Components of a Simscape Multibody Model [8]

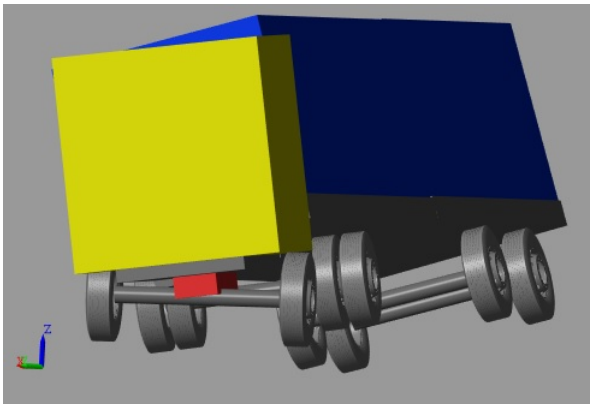

Figure 3.2: Rollover of 4 axle Tractor Semitrailer visualized in the Mechanics Explorer

3.2 Tractor Semitrailer Model

The model of the tractor semitrailer can be subdivided into 3 main modules. The driver module, the tractor module and the semitrailer module. These modules and the purpose they serve are described below:

Driver Module

The driver of a vehicle provides the input to navigate the vehicle in a specific manner. Similarly, the driver module is designed to provide the necessary steer, throttle and brake input so as to make the vehicle follow the trajectory requested. The steer input can be specified either directly as an array before the initialization of the model or can be converted into the coordinates that a path following controller will attempt to follow. One can choose how to provide the steer input in the initialization code. More about the path following controller

will be described in subsection 3.2.1. The throttle input to the vehicle is controlled using a cruise controller, which is a PI controller to follow the reference velocity specified during model initialization.

Tractor Module

The tractor module defines the positions of the body elements that make up the tractor. They are: the cabin, engine block, chassis elements, the steer axle, the drive axle and wheels. The position of all these parts are specified using rigid transforms. The world frame, solver configuration and mechanism configuration of the model are present in this module. The main dimensions that are needed to specify the geometry of the tractor, wheelbase, initial axle loads, mass of chassis elements, are defined in the mask of the model. The chassis is divided into 2 parts and connected with a revolute joint oriented in the longitudinal direction, where a stiffness is specified. This is done to model the torsional stiffness of the chassis. The cabin block in the tractor module contains the cabin body. On the front surface of this cabin body, the aerodynamic drag force is defined. More on this will follow in a later section. The drive-line block converts the throttle input from the driver model into the drive torque that acts at the wheels. The drive-line model is also able to calculate the gear shifts the tractor will make during its operation and also calculate the fuel consumption. The improvements made to the drive-line model will be elaborated later. The axles are connected to the chassis using a system of springs and dampers for each wheel, whose stiffnesses are specified in the mask of the axle module.

Semitrailer Module

The semitrailer module defines the positions of the body elements that form the semitrailer. They are: the 5^{th} wheel location, the chassis elements of the trailer, the load elements of the trailer, and the trailer axles and their wheels. The position of all these parts are defined by connecting one frame to another using rigid transforms, whose values are initialized in the mask of the module and the blocks within the module. The trailer chassis and load are also divided into 2 parts, and connected using a revolute joint in the longitudinal direction, to model the torsional stiffnesses of both the chassis. The main dimensions that define the geometry of the trailer, 5^{th} wheel position, position of axles, chassis length, mass and density of load, initial axe loads, can be input into the mask of the trailer module. The 5^{th} wheel is modelled using a combination of 2 revolute joints oriented along the y and z axis. This makes the 5^{th} wheel restrict the translational degrees of freedom, while allowing pitch and yaw motions. This also couples the roll of the semitrailer to the tractor. The axles of the trailer are also connected to the chassis via a system of spring and dampers.

3.2.1 Modifications made to the original model

The original model had been made in Simscape Multibody based on the Sim-Mechanics version of the tractor semitrailer of the TU/e Commercial Vehicle Library. The TU/e Commercial vehicle library allows users to assemble the different types of heavy goods vehicles. More about the TU/e CVL can be found in [18][9].

To make the original model capable of providing a proper comparison between the 2 axle semitrailer and the 3 axle semitrailer, certain modifications are made to the original model.

Rear Axle Steering

The rear axle of the 2 axle semitrailer needs a steering input at the rear axle that will aid in the manoeuvrability of this vehicle combination. The mechanism through which the steer-input is provided to the rear axle is Command Steering. In command steering of a multiple axle trailer system, the steered axles are provided a steer angle that is proportional to the articulation angle between the tractor and the trailer unit. The steering input is derived through geometric relationships formed by the dimensions of the vehicle and the articulation angles developed. The idea is to place all tractor and trailer non-steered axles on a circular path and steer the rearmost axle of the 2 axle semitrailer so that they share a common instantaneous center of zero velocity. Such a steering mechanism will improve the low speed manoeuvrability.

The assumptions made to derive the steer angle for the rear axle are shown next:

1. The orientation of the tractor-semitrailer is such that the articulation angle is ψ_1
2. The rear axle of the tractor and the front axle of the semitrailer are not steered and hence are perpendicular to the center-line of their respective bodies.
3. Due to the articulation angle, the line extended from the rear axle of the tractor and the line extended from the front axle of the semitrailer must intersect at the instantaneous center of zero velocity O.

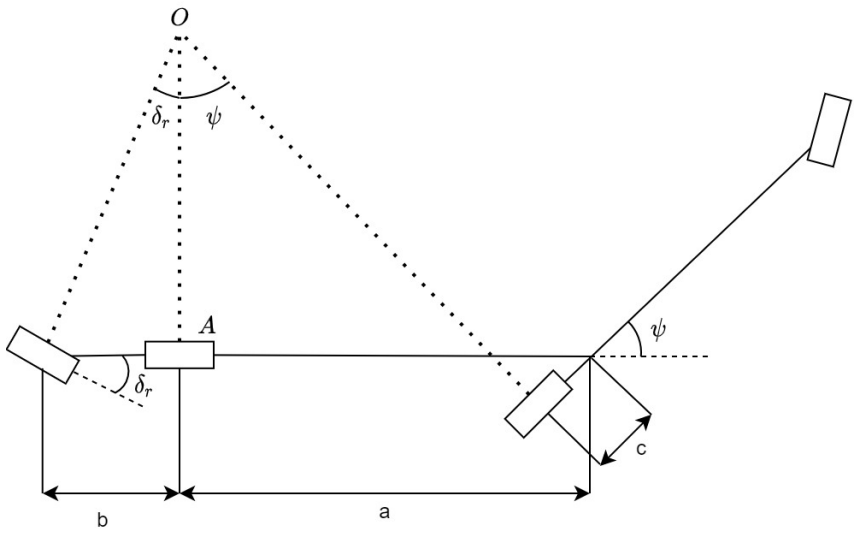

Figure 3.3: Single track model of 2 axle semitrailer when cornering

From the geometry of the triangles formed in Figure 3.3, the steering angle of the rear axle δ_r can be derived as:

$$\delta_r = \arctan\left(\frac{b\tan\psi}{a - \frac{c}{\cos\psi}}\right) \tag{3.1}$$

The complete derivation of the steering angle can be referred to in Appendix D.

The articulation angle is measured using a transform sensor, attached to the revolute joint at the location of the 5^{th} wheel. This articulation angle is fed to a MATLAB function block, where (3.1) is implemented. This provides the necessary steer angles to the wheels of the rear axle.

Path Following Controller

Depending on the manoeuvre, one can choose to either define a steer input to the steer axle wheels as a function of time or to guide the vehicle along a prescribed path using path following. When evaluating performance using high speed manoeuvres such as the single sine lane change, the steer input is defined as a function of time, whereas a low speed manoeuvre such as the EU 360° turn uses the path follower which can make corrections to the path whenever a deviation from the desired trajectory is detected.

The path following controller works in the following manner. First, the desired vehicle trajectory is defined, where the prescribed path in the global (x,y) coordinate system is defined. The longitudinal and lateral positions of the vehicle are monitored continuously and compared with the desired path as the simulation progresses. As the deviation from the prescribed path increases, the steer angle is adjusted to keep the vehicle in the prescribed path. The concept that the path following controller utilizes is shown in figure 3.4.

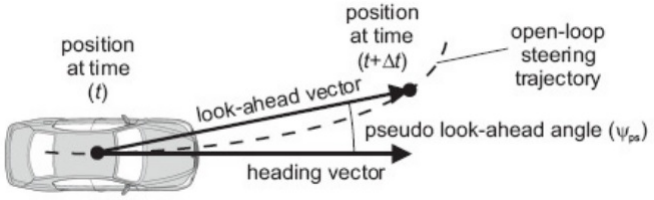

Figure 3.4: Concept of Path Following Controller [9]

The path following block is implemented such that the controller calculates the error from the prescribed path at a certain look ahead distance, and corrects the steer angle based on the error generated. The steer angle that is applied is calculated as:

$$\delta_t = c_1 \cdot \psi_{ps} \tag{3.2}$$

where c_1 = steering sensitivity and ψ_{ps} = look ahead angle

Aerodynamic Force

The air drag experienced by a tractor semitrailer is due to air flow caused by the frontal

area of the vehicle. The equation that governs the aerodynamic drag force that acts on a body is given by:

$$F_{aero} = \frac{1}{2}\rho A_f C_d V^2 \tag{3.3}$$

where ρ is the density of air and A_f is the frontal area of the tractor and C_d is the drag coefficient.

The frontal area A_f of the tractor equals 10.5 m/s^2[33] and the density of air ρ equals 1.225 kg/m^3.

More information on the determination of the air drag coefficient can be found in the Appendix C of [33].

The aerodynamic force is incorporated in the model. The velocity of the cabin is measured using a transform sensor, and the aerodynamic drag force is calculated using (3.3). This aerodynamic force is then sent to an external force and torque block, which generates the aerodynamic force in a direction opposite to the velocity of the vehicle, at the geometric center of the front face of the cube that represents the cabin.

Ackermann Steering

During testing of the vehicle along a steady state low speed turn, it had been found that equal and opposite slip angles are being generated at the wheels of the steered axles. This is due to the fact that equal steering input is provided to both the left and right wheels. In road vehicles, the inner wheel is always steered sharper than the outer wheel during a turn to reduce tire slippage. This is known as Ackermann Steering.

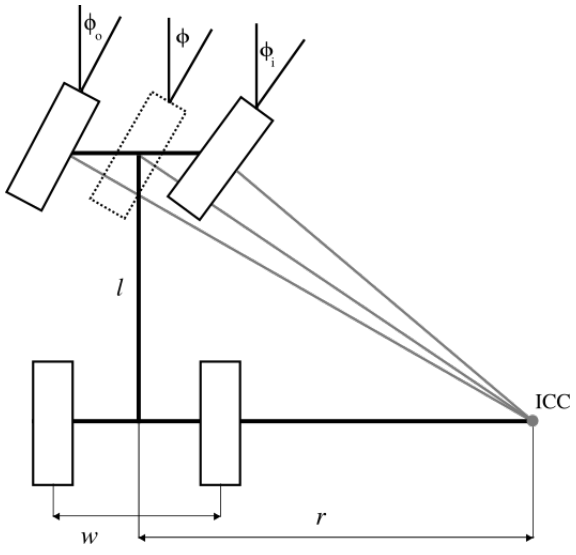

Figure 3.5: Ackermann Steering [10]

Figure 3.5 illustrates Ackermann Steering. Here, w is the track width, l is the wheelbase, ϕ_i is the relative steering angle of the inner wheel, ϕ_o is the relative steering angle of the outer

wheel and r is the distance between ICC and center of vehicle. The Ackermann steering angles can then be derived by considering the 3 triangles formed and expressed as shown below:

$$\tan\phi = \frac{l}{r} \tag{3.4}$$

$$\tan\phi_i = \frac{l}{r - \frac{w}{2}} \tag{3.5}$$

$$\tan\phi_o = \frac{l}{r + \frac{w}{2}} \tag{3.6}$$

The steering angle formulae are input in a MATLAB function block, whose output is the steering angle to both the left and right wheels. After the function had been implemented, the slip forces at the steered axles are relatively equal and in the same direction. This applies for the slip angles too.

Drive-line Model

The drive-line block in the original model had a relatively simple representation of an engine. The engine has been represented by a function block where the total engine power (330 kW) is divided by the product of the instantaneous angular velocity at the wheels times final drive ratio to get the engine torque. This approach is sufficient when doing performance based tests, but cannot be used to make fuel consumption calculations. The original drive-line block assumes that the engine is connected to a continuously variable transmission. This is not how a tractor operates in reality and alterations are made to this block.

In order to make fuel consumption calculations the following elements have been added.

- Gear ratios are specified.
- A conversion to make the instantaneous power generated at the wheels into what gear the tractor would be operating in. This would depend on the velocity and the power at the wheels at that instant.
- There needs to be a fuel consumption map, which uses engine torque and rpm to calculate the instantaneous fuel consumption rate.

The forward power-train model mentioned in the work of Parfant [33] is used as a base from which the driveline model is developed. The gear ratios used are from the data sheets [34] and [35] and an assumption is made, that the tractor has a 16 speed gearbox from ZF. Constant transmission efficiency is assumed for each gear as it is often done for fuel consumption calculations [36].

A gear shift strategy is implemented, which is based on maximum efficiency of fuel consumption. This is done by an offline minimization function which calculates the optimum gear ratio the vehicle should operate in, based on the brake specific fuel consumption data of a generic 330 kW diesel engine. The output of this function is a shift-map, which is a 2 dimensional lookup table, that generates the gear the vehicle should operate in to get the

Table 3.1: Engine and Transmission Parameters

Parameter	Unit	Value	Reference
Engine Type	[-]	MX - 13 (Euro-6 Diesel)	[34]
Max. Engine Power	[kW]	330	
Max. Engine Torque	[Nm}	2221	
Number of Gears	[-]	16	[34]
Range of Gear Ratios	[-]	14.12 - 0.83	[35]
Final Drive Ratio	[-]	3.07	

lowest fuel consumption. The inputs to the shift-map are the wheel torque and forward velocity. The shift-map generated is shown in the figure 3.6a. Note that the fuel consumption reported by the method used here is most suited to constant speed operation. It is mentioned in reference [33] that the map may not be very accurate at low engine speeds.

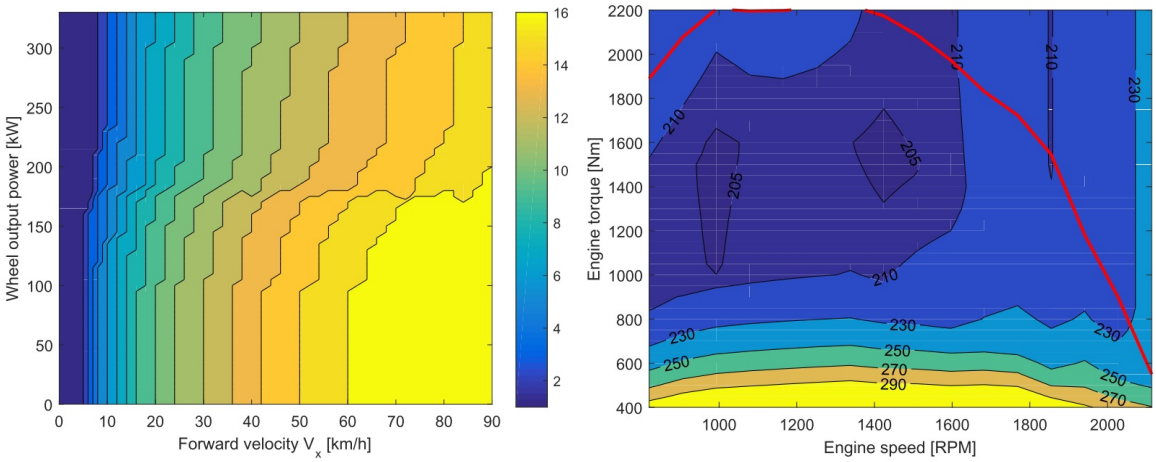

(a) Shift map [33]

(b) Torque Map [33]

Figure 3.6: Shift Map and Torque Map used in Driveline Model

A two-dimensional lookup-table, which is a function of engine speed ω_{ICE} and torque τ_{ICE}, is used to generate the fuel mass flow rate $\dot{m}_f$. The generic fuel map of the 330 kW Euro 6 diesel engine, obtained from [33], is used here. The Torque map with BSFC is shown in figure 3.6b. The red line shown in figure is the engine torque limit as a function of engine speed. This mass flow rate is then integrated over time to get the fuel consumption. Also, the powertrain parameters are based on data sheets of a DAF XF460 tractor. A clutch model and a differential are not implemented to maintain simplicity of the model. Equal torque split is maintained at both sides of the drive axle.

The operation of the powertrain model is explained next. The inputs to the drive-line block are the wheel velocity and the throttle input. The wheel velocity is multiplied with the radius of the tyre to get forward velocity. The instantaneous power at the wheels is obtained by multiplying the drive torque with the wheel angular velocity. Both velocity and power

at wheels are fed to the shift map, which generates the number of the gear that the tractor should operate in for the lowest fuel consumption. This is then fed to a shifting time block, which ensures that abrupt gear changes do not occur when the input variables to the shift map are near boundary values. The signal is then fed to a 1D lookup table, which converts the gear number to the gear ratio of the 16 speed gearbox multiplied with the final drive ratio. The gear ratio times final drive ratio is then multiplied with the average wheel speed to get the engine speed at that instant. The engine speed is fed to a function that divides the peak power of the engine with the obtained engine speed signal to get the engine torque. This engine torque is then fed to the fuel map along with engine speed to get the mass flow rate of fuel at that time (gram/s), and this is integrated and divided by 1000 to get the fuel consumption in liters. To get the wheel torque, the engine torque is multiplied with the product of the instantaneous gear ratio and final drive ratio, and is split evenly over both driven wheels. Appendix G shows the implementation of the new drive-line block.

A picture of the shifting time block that can be seen as a part of the updated power-train model is shown in Figure 3.7.

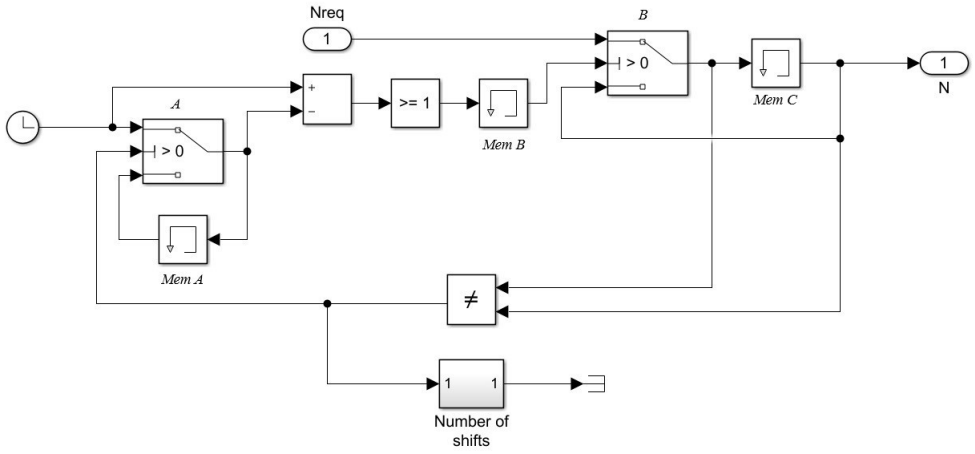

Figure 3.7: Shifting Time block

The inputs to the shifting time block are the simulation time and the required gear shift at a time instance. As time continues to progress in the simulation, the net effect of the shifting time block is that gear shifts can occur only after a minimum time delay of at-least 1 second. This ensures that the gear shift from the shiftmap can only affect the torque and engine speed of the engine when the shiftmap outputs a different value of the required gear shift after more than a second. The shifting time block is a safety measure to prevent rapid gear changes, which can affect the fuel consumption calculations.

Static Axle Loading

An objective of this thesis is to make the simulation model as close as possible to a tractor semitrailer in real life, so that the results found in the simulation environment can be used to make decisions on real world applicability. The vehicle models should have the same static

axle loading in simulation and in reality. Since the dimensions of the vehicles are the same, this would ensure that the vehicle in the simulation environment generates the slip forces similar to real life. Thus, only if the static axle loading matches, will the performance comparison of the trailers yield accurate results. The dimensions of the 5 axle and 4 axle tractor semi-trailers are displayed in Figure 3.9.

To get the axle loading according to the vehicle specification, the following changes are made to the original tractor semitrailer model.

- The dimensions of the trailer play a role in the static axle loading of the vehicle. The initial vertical axle loading of the trailers are obtained according to the dimensions shown in Figure 3.9. The excel sheet with the calculations of the initial axle loads are provided by Knapen Trailers and these values are used in the model along with the tractor and trailer dimensions to get the appropriate values of the unloaded height of the spring and dampers between the axles.
- The position of the center of gravity of the trailer chassis affects the distribution of axle loads in the model. This is due to the fact that each individual axle is connected to the trailer using 2 sets of springs and dampers and is sensitive to the proportion of the load that is directly atop the axle. Trailers in real life have air suspensions which equalize the load acting on each axle, irrespective of the placement of the CG of the chassis. The CG is shifted by altering the percentage of mass distribution of the front and rear chassis element such that equal axle loading is obtained across the trailer axles.

The static axle loading of the tractor semitrailer combinations that are compared are listed in Tables 3.2 and 3.3. More information on the dimensions of the trailer combinations can be found in Figure 3.9.

Axle	**Load [kg]**
Steer Axle	7450
Drive Axle	11550
Trailer Axle 1	7000
Trailer Axle 2	7000
Trailer Axle 3	7000
Total	40000

Table 3.2: 5 axle Tractor Semitrailer

Axle	**Load [kg]**
Steer Axle	8450
Drive Axle	11550
Trailer Axle 1	10000
Trailer Axle 2	10000
Total	40000

Table 3.3: 4 axle Tractor Semitrailer

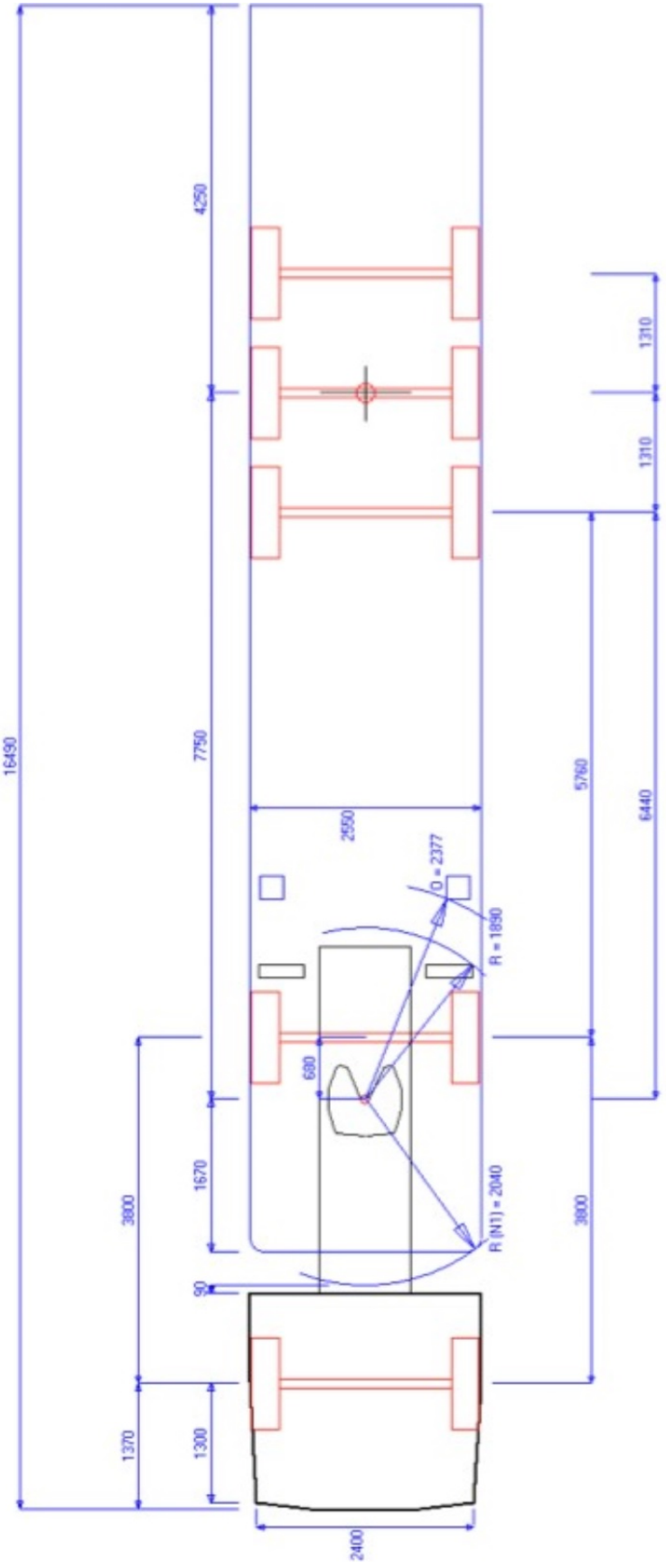

Figure 3.8: Dimensions of 5 axle tractor semi-trailer

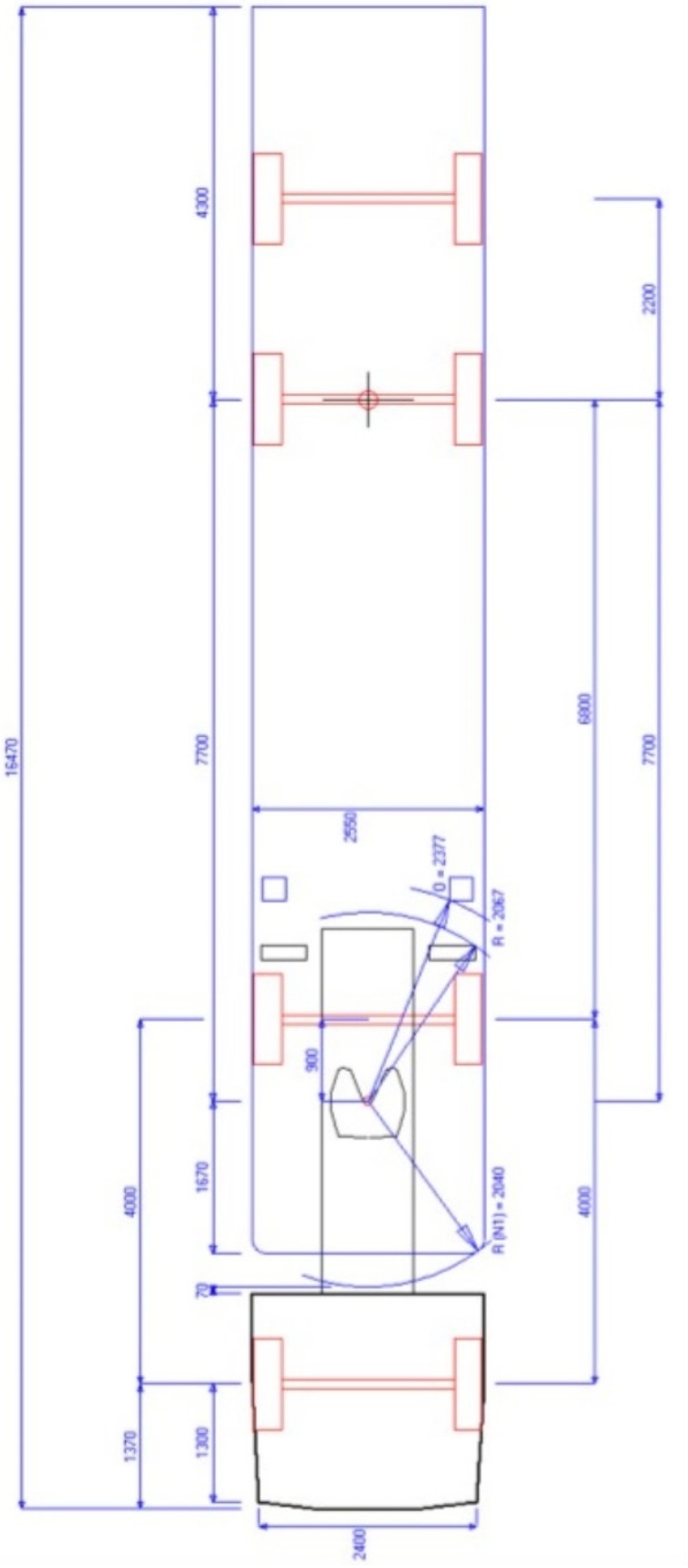

Figure 3.9: Dimensions of 4 axle tractor semi-trailer

3.3 Summary

This chapter begins with a description of the simulation environment of Simscape Multibody, using which the models of the tractor semi-trailers were created. Next, a general description of the various modules that are a part of the tractor semi-trailer model along with their functionality is provided . Then, light is shed on the various elements of the model that have been added as an effort of this thesis work. The implementation of rear axle steering, aerodynamic drag force, ackermann steering and the updated driveline model are described. Finally, the methodology used to obtain the static axle loading of the compared tractor semi-trailers is described.

Chapter 4

Rolling Resistance and Fuel Consumption

The main factors that affect the fuel consumption during straight line driving on a level road are aerodynamics and rolling resistance of the vehicle. This chapter will describe the steps taken to get representative rolling resistance forces for both the tractor semitrailer combinations that are compared. There after, the procedure to determine the fuel consumption will be described. Finally the results and conclusions that can be drawn from the results will be presented.

4.1 Rolling Resistance

The origin of rolling resistance is due to the visco-elastic property of the tires. The deformation of the tyre causes the flattening of the contact patch when it rolls. This dissipates energy in the form of heat. Rolling resistance can be defined as the energy consumed by the tire per unit distance covered [11]. It is expressed as a force and is characterized by the equation:

$$F_{RR} = C_{RR} \cdot Z \tag{4.1}$$

where C_{RR} is the rolling resistance coefficient and Z is the normal load acting on the tyre.

There are many external factors that affect rolling resistance. The most prominent factors will be described next.

- **Tyre Pressure:** It is common knowledge that when the tire pressure is increased, the rolling resistance of the tyre decreases. Increase of tyre pressure increases the compression of the tread blocks, but prevents their bending and shearing. [11] This means that the driving force from the axle is more effectively transferred to the ground. The rolling resistance coefficient is dependent on tire pressure, as can be seen from Fig. 4.1.

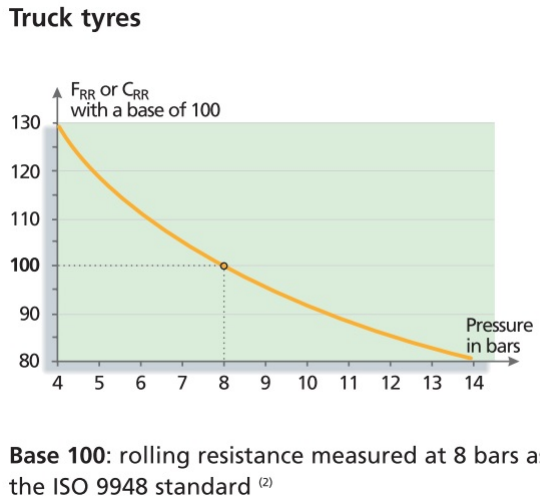

Figure 4.1: Pressure vs rolling resistance coefficient [11]

- **Load:** The rolling resistance coefficient C_{RR} decreases slightly as load increases. A greater normal load on the tyre implies that more work is done by the tyre during its motion along the same travelled distance. This means that there is greater dissipation of energy from the tyre to the road as the rubber molecules stick to the pavement more, leading to an increase in tyre temperature at the contact patch. Since the vertical dynamics of the tyre on the road is represented by a spring damper system, the increased temperature decreases the spring constant of the tyre as the molecules of rubber have more energy to adjust to the aberrations of the pavement. This means that the visco-elasticity of the tyre decreases as temperature increases, reducing the rolling resistance coefficient. However, the total rolling resistance force (F_{RR}) increases with load as the contribution of the normal load is greater. The dependency of C_{RR} and F_{RR} can be seen in the Fig. 4.2.

Other factors, such as speed, ambient temperature and rolling time of the tyre, also affect the rolling resistance coefficient. However, tire pressure and other factors are not included in our analysis due to the following reasons. Even-though the effect of tyre pressure changes are modelled in the Swift Tyre Model used in the model of the Tractor Semitrailer, the dependency of the rolling resistance coefficient on the tyre pressure is tyre specific. This dependency wasn't known for the tyre used in this thesis. It is assumed that Tyre Pressure does not change over time. Tractor Semitrailers do not reach speeds of 120 km/h. In the Netherlands, Trucks and vehicles above 3.5 tons are required to have a speed limiting device to prevent them from speeding above 90 km/h [37]. Ambient temperature and tyre temperature are not parameters that are simulated in the Simscape Multibody. It is assumed that the temperature remains constant during each simulation.

The effect of tyre pressure and load on rolling resistance can be described by the following empirical formula:

$$F_{RR} = k \cdot P^{\alpha} \cdot Z^{\beta} \tag{4.2}$$

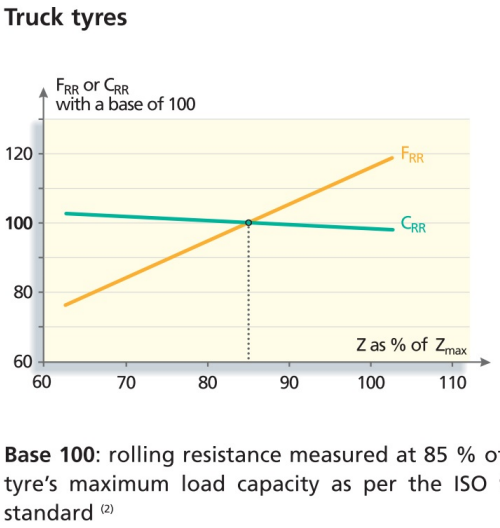

Figure 4.2: Load vs Coefficient of Rolling Resistance & Rolling Resistance Force [11]

where k = constant for a given tyre and for a truck tyre designed for motorway use: $\alpha \approx -0.2$ and $\beta \approx 0.9$. [11]

The effect of the vertical force on rolling resistance equals:

$$F_{RR} = F_{RR-ISO} \cdot (\frac{Z}{Z_{ISO}})^{\beta} \tag{4.3}$$

where Z_{ISO} and F_{RR-ISO} are the rated load and rolling resistance force for a given tyre.

From (4.3) and (4.1), we can get the following dependence of the coefficient of rolling resistance C_{RR} on the vertical force Z. The derivation of this equation is elaborated in Appendix E.

$$C_{RR} = C_{RR-ISO} \cdot (\frac{Z}{Z_{ISO}})^{1-\beta} \tag{4.4}$$

To get representative values for the rolling resistance coefficient, two premier tyre manufacturers had been contacted. These values had been provided for Steer Axle, Drive Axle and Trailer Axle tyres that are used for both regional distribution and long haul driving. The average of the values of each tyre type are determined and listed in Table 4.1.

Now, using (4.4) and the load acting on each axle, as mentioned in Table 3.2, the corrected coefficient of rolling resistance can be obtained for the tractor semitrailer combinations.

To check the rolling resistance values, a roll-out test had been simulated. In this test, the aerodynamics module had been switched off and the tractor semitrailer is accelerated from 50 km/h at full throttle for 10 seconds. Thereafter, the vehicle had been allowed to roll freely. Thus, the only force that resists the forward motion of the wheels is the rolling resistance force. Now using (4.1) and Table 3.2, the rolling resistance force for each wheel can be calculated. Slight adjustments have been made to the rolling resistance coefficients by repeating

		Tyre Type	Tyre Size	Z_{ISO} [T]	C_{RR-ISO}
Regional Distribution	Tractor	Steer Axle	315/70 R22.5	4.0	5.6
			385/65 R22.5	4.5	5.6
		Drive Axle	315/70 R22.5	3.8	6.2
	Trailer	9 ton axle	385/65 R22.5	4.5	4.9
		10 ton axle	385/65 R22.5	5.0	4.9
Long Haul	Tractor	Steer Axle	315/70 R22.5	4.0	5.3
			385/65 R22.5	4.5	5.3
		Drive Axle	315/70 R22.5	3.8	5.7
	Trailer	9 ton axle	385/65 R22.5	4.5	4.2
		10 ton axle	385/65 R22.5	5.0	4.2

Table 4.1: Average Rolling Resistance Coefficients used in model

the roll-out test so that the rolling resistance forces are almost equal to the calculations made.

The total rolling resistance force of both vehicle combinations are shown in Table 4.2 for both regional and long haul tyres. The rolling resistance forces are listed at zero payload, 50 % payload and maximum payload. The values of total rolling resistance are quite close to one another for both the regional distribution and long haul tyre types. This is a first indication that the advantages in Fuel Consumption from the trailer this thesis proposes will not be very high in a straight line when both vehicles share the same gross vehicle weights in the fully loaded condition.

Vehicle Type	**Rolling Resistance Force (N)**	
	Regional Distribution tyres	**Long Haul tyres**
	Max Payload (25 ton - 5 axle TS and 26 ton - 4 axle TS)	
5 axle Tractor Semi-trailer	2160	1930
4 axle Tractor Semi-trailer	2105	1890
	12.5 ton Payload	
5 axle Tractor Semi-trailer	1515	1360
4 axle Tractor Semi-trailer	1455	1315
	Zero Payload	
5 axle Tractor Semi-trailer	850	770
4 axle Tractor Semi-trailer	795	725

Table 4.2: Rolling resistance forces of tractor semi-trailers

As a rule of thumb, it can be stated that for tractor semitrailers the aerodynamic forces reach the same magnitude as rolling resistance forces at speeds of about 80 km/h. The magnitude of power to overcome aerodynamic drag reaches a magnitude equal to that of the power to overcome rolling resistance force at 83 km/h for vehicles with regional distribution tyres and 80 km/h for vehicles with long haul tyres, as shown in Figures 4.3a and 4.3b.

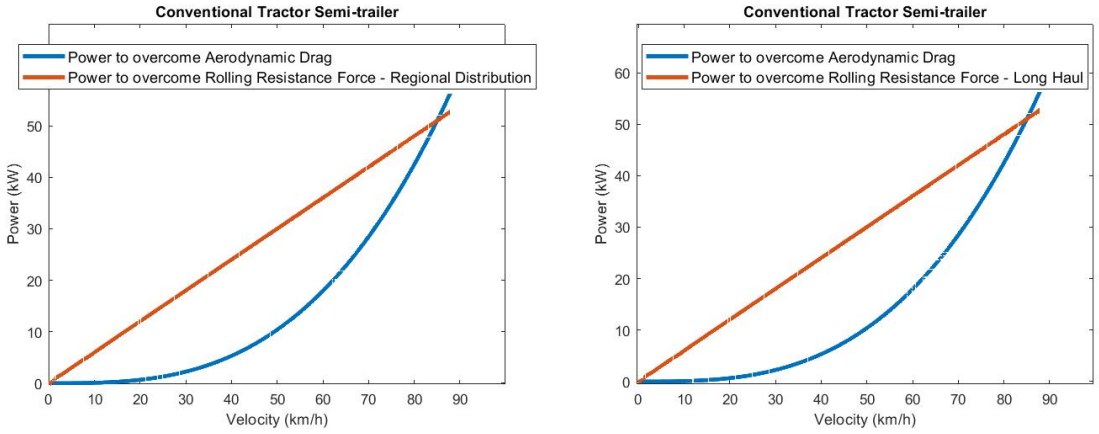

(a) Regional Distribution tyres

(b) Long Haul tyres

Figure 4.3: Power to overcome Aerodynamic drag and Rolling resistance force (5 axle tractor semi-trailer)

4.2 Fuel Consumption

The potential benefits that the proposed 2 axle semitrailer can give in fuel consumption are instrumental in deciding whether the shift from the 3 axle semitrailer is worth the effort needed to change the EU legislation. The fuel consumption is calculated for two conditions:

- Straight Line Driving
- Driving in a Circle

4.2.1 Straight Line Driving

In this test the vehicle travels in a straight line at a constant speed. The simulation is stopped when the vehicle has covered 1 km of travelled distance. The vehicle speeds had been varied from 50 km/h in increments of 10 km/h till 80 km/h. When travelling in a straight line, the forces that resist the motion of the vehicle are the rolling resistance force and the aerodynamic drag force. At a constant velocity, the aerodynamic drag force is a constant. This makes the differences in rolling resistance force the only variable that affects the fuel consumption in these tests. The tests are indicative of two types of differences in fuel consumption.

- Reduction in fuel consumption due to lower rolling resistance force between 5 axle semi-trailer and 4 axle semi-trailer due to the 4 axle semi-trailer having lesser number of tyres carrying more load.
- Difference in fuel consumption between the regional distribution tyre variant and the long haul tyre variant.

To ensure that a complete picture of the variation of fuel consumption with loading condition is obtained, the tests are repeated at 0%, 50% and 100% total payload. The results of the tests are tabulated in Appendix A. The average fuel consumption over the different constant

speeds of operation are plotted with respect to the total payload in Figure 4.4

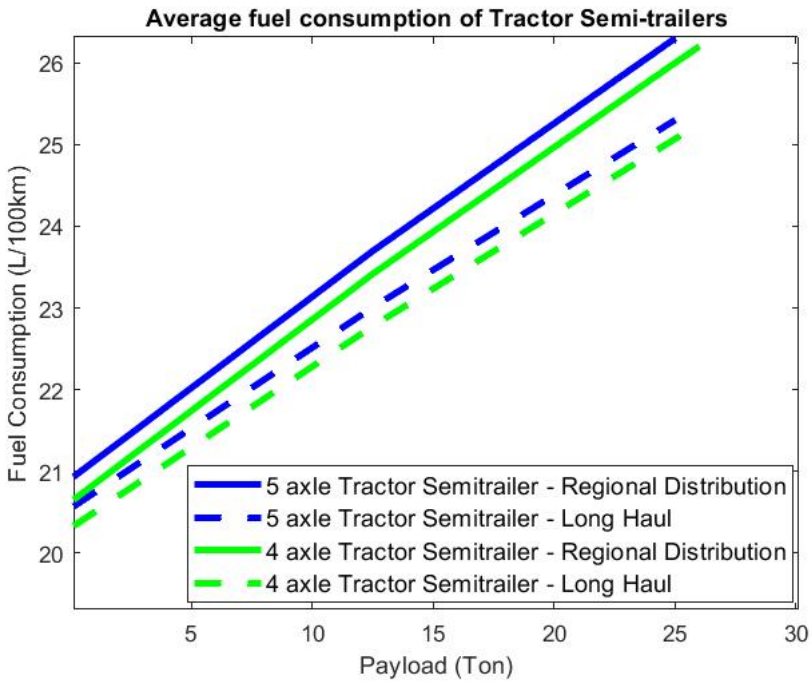

Figure 4.4: Average fuel consumption of tractor semi-trailers

The vehicle equipped with long haul tires show a considerable decrease in fuel consumption compared to the regional distribution tires. This is expected due to their lower rolling resistance coefficient. From the results of both regional and long haul tires, it can be seen that the difference in fuel consumption continues to decrease between the semi-trailer types as the gross vehicle weight of the vehicle increases. The difference in fuel consumption at 0 payload is due to the fact that the 2 axle semitrailer is 1000 kg lighter in weight. At the condition of 0% payload, the gross vehicle weights are 15 ton and 14 ton for the 5 axle and 4 axle tractor semitrailer respectively. The percentage difference in fuel consumption on average for the 0% payload condition is 1.34%. The difference in fuel consumption at the fully loaded condition is minimal, at 0.25%. When the 2 axle semi-trailer is used over the conventional tractor semi-trailer for straight line constant speed driving, one can see a 0.25% to 1.7% improvement in fuel consumption depending on the loading scenario and velocity.

The fuel consumption had also been evaluated on a per ton km basis to fully realize the performance advantage offered by switching to the 2 axle semitrailer. The payloads of 12.5 ton, 25 ton are considered for the conventional tractor semi-trailer representing half load and full load conditions and payloads of 12.5 ton, 25 ton and 26 ton are considered for the 4 axle tractor semi-trailer to provide an equivalent comparison. The results are presented in Tables 4.3 and 4.4. It can be seen that on average, the percentage difference between the 2 trailer types are 4.4% for regional distribution tires and 4.2% for long haul tires. The ability to add another 1000 kg of payload improves the specific fuel consumption considerably. The 2 axle trailer will yield substantially lower fuel consumption on a per ton km basis.

5 axle Tractor Semi-trailer	Fuel Consumption [L/ton.km]			
	Regional distribution tyres		Long haul tyres	
	Payload (ton)		*Payload (ton)*	
Speed (km/h)	**12.5**	**25**	**12.5**	**25**
50	0,0151	0,0086	0,0145	0,0082
60	0,0178	0,0099	0,0172	0,0095
70	0,0204	0,0113	0,0198	0,0108
80				

Table 4.3: Fuel Consumption [L/ton.km] for 5 axle tractor semi-trailer

4 axle Tractor Semi-trailer	Fuel Consumption [L/ton.km]					
	Regional distribution tyres			Long haul tyres		
	Payload (ton)			*Payload (ton)*		
Speed (km/h)	**12.5**	**25**	**26**	**12.5**	**25**	**26**
50	0,0149	0,0085	0,0082	0,0144	0,0081	0,0079
60	0,0175	0,0098	0,0095	0,0170	0,0094	0,0091
70	0,0202	0,0111	0,0108	0,0197	0,0108	0,0104
80	0,0224	0,0122	0,0118	0,0219	0,0118	0,0114

Table 4.4: Fuel Consumption [L/ton.km] for 4 axle tractor semi-trailer

4.2.2 Driving in a circle

Fuel Consumption is also calculated when the tractor semi-trailer model does the EU 360° turn. The tractor semitrailer is driven in a circle of outer radius 12.5 m at a speed of 7.5 kph. Once a steady state circular turn had been established, the fuel consumption is determined. The turning manoeuvre had been conducted five times. To understand the extent of the reduction in fuel consumption when driving in a circle, the test had been conducted at 0 ton payload, 12.5 ton payload and 25 ton payload.

The difference in fuel consumption performance comes from the fact that the 3 axle tractor semitrailer differs from the 2 axle semitrailer in the way slip angles develop on the trailer axles. This can be observed from the figure 4.5. The generation of the slip angles on the first and third axle of the semitrailer induces lateral forces that the tractor will need to overcome to orient the trailer in the direction of the 5^{th} wheel. This induces the need for more power from the engine to drive the trailer in a circle. The 2 axle tractor semitrailer on the other hand, does not develop large slip angles due to steering of the rear axle. This means that the 5^{th} wheel forces that act on the tractor, as a result of lateral forces at the trailer axles during the EU 360° are smaller. This advantage can be clearly seen in the results of the fuel consumption presented in Table 4.5.

The results show that the 5 axle tractor semi-trailer has a fuel consumption that is between 2 to 3 times that of the 4 axle tractor semi-trailer during a very tight steady state circle depending on the loading condition. There is a drastic improvement in performance when using the 2 axle semi-trailer with rear trailer axle steering. Routes with a large number of turns may benefit from the reduction in fuel consumption that the 2 axle trailer can provide.

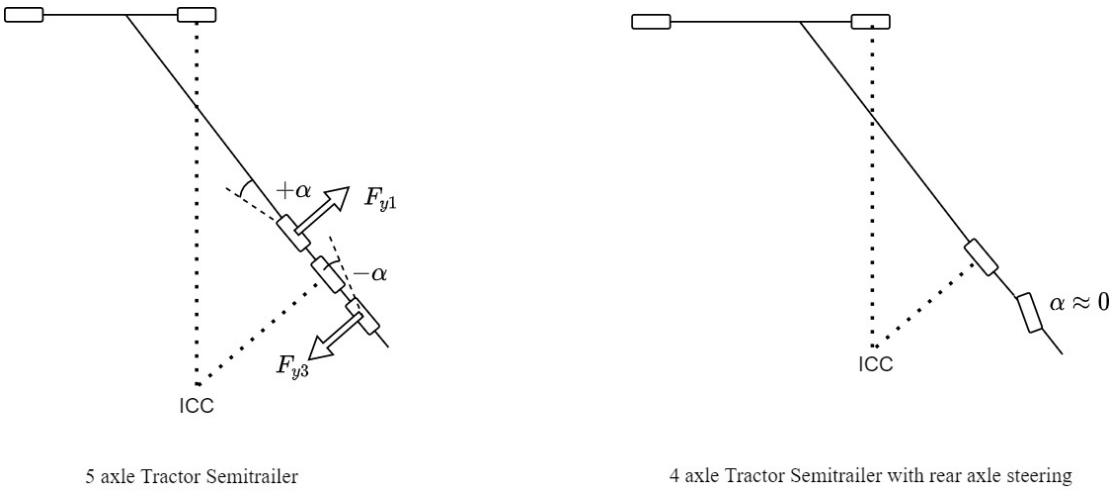

Figure 4.5: Difference in the development of slip angles for Trailers

Vehicle Type	**Fuel Consumption [L/100km]**		
	Payload (ton)		
	0	**12.5**	**25**
5 axle Tractor Semi-trailer	44.68	71.68	91.53
4 axle Tractor Semi-trailer	23.56	28.46	33.2

Table 4.5: Fuel Consumption during EU 360° Circle

4.3 Summary

This chapter begins with a brief description of the various factors that affect the calculation of fuel consumption. The section on rolling resistance explores the underlying phenomena that causes rolling resistance and the relationships that exist with the relevant parameters. The procedure used to get values of the rolling resistance coefficients on the tractor semitrailer model is described. Testing to evaluate the fuel consumption reduction had been done for the scenarios of straight line driving and driving in a circle. The results show that on a per ton of payload basis [L/ton.km], the 4 axle semitrailer improves the fuel consumption by ≈ 4.3 as the 4 axle tractor semitrailer has a maximum payload capacity of 26 tons which is 1000 kg more than that of the 5 axle tractor semi-trailer. The subsequent subsection mentions the performance gains obtained when operating the tractor semitrailer in a circle. The great reduction of side slip forces reduces the fuel consumption of the tractor semitrailer in a circle by almost 50 to 67% depending on the loading condition. The 4 axle tractor semitrailer will in general offer considerable reductions in fuel consumption. In a straight line, these reductions are comparatively small. There is a much larger reduction in fuel consumption when turning in a tight circle.

Chapter 5

Tire Wear

The state of tyre wear on a vehicle play a huge role in its manoeuvrability and safety over a period of time. Designing tires that are safe, fuel efficient and long lasting requires an in-depth understanding of the tribology of tire road interaction [5]. One of the goals of this thesis is to quantify the level of tire-wear that occurs during certain manoeuvres. A literature study has been conducted with the aim of finding a middle ground in describing the behaviour of tire-wear with sufficient accuracy. This section will describe the methodology used to gauge the level of tire-wear between the tractor semitrailer configurations. The results obtained using these calculations are presented and conclusions are drawn from them.

5.1 Literature Review

It is clear that simple analytical models based on normal pressure distribution and sliding distance covered by a tread element can represent tire wear, as can be seen from Archard's wear law and Schallamach wear law. However these models do not represent the joint effect of load and slip angle. Also, the application for which these laws are designed are for wear of metal disks etc, whose mechanical properties are quite different from the visco-elasticity that tires possess. Thus, these laws can not accurately predict tire wear.

Building completely analytical models that predict tire wear is very challenging, as wear depends on many factors such as the dynamics of the tyre and the vehicle, the mechanical contact conditions and tyre-road interaction, temperature and pressure effects and structure of the tyre and material properties (e.g. hardness, damping, abrasion characteristics). The work of Li et al [3] is a parameter sensitivity study of the factors that affect tire wear. Most prominent factor is the slip angle. Speed and sprung mass also exert an influence of comparable magnitude, but these effects are included when the tire wear is measured as a result of the slip forces that are generated. Hence, it had been decided that slip forces would be the key to determining the effect of tire wear.

Tire-wear occurs across mainly 2 events during the operation of a heavy goods vehicle such as a tractor semitrailer, being straight line acceleration and braking and scrubbing of tires during turning [5].

Of these factors, the instances where a tractor semitrailer generates enough braking or

acceleration to result in wheel lock or spin do not occur as frequently in the lifetime of the trailers operation as does the effect of scrubbing of tires during a turning manoeuvre. This is the approach taken by David Cebon et al. [5], where a method to empirically estimate the tire-wear of a particular heavy goods vehicle tyre is described. In this work, tyre wear had been measured at eight different slip angles, between 0° to 14° with a normal load of 100 kN per axle. The testing had been done on an asphalt test track, which is meant to represent the average road condition in the EU. The measurements showed that the tire-wear behaviour can be represented by a simple quadratic (2.8). Then using (2.9), one can obtain the mass of the tyre (in grams) that wore off during that manoeuvre. This approach has been taken as a base from which the method to calculate tire-wear is obtained.

It is to be noted that the results drawn from the methodology described in the next section is at best be an approximation. Tire wear occurs due to a wide variety of factors, road surface, friction level, angularity of the particles, humidity, ambient temperature, which are too complex to be included into the Tractor Semitrailer model. Also, tire wear varies heavily with the type of tire that is used. Regional distribution tires with a higher coefficient of rolling resistance are made more resistant to tire-wear due to scrubbing, while long haul tyres will wear more during scrubbing. The performance improvement in terms of tire-wear when using the proposed 2 axle semitrailer can be compared to that of the 3 axle semitrailer, assuming that all other factors that affect tire wear remain constant. This would be a first step in giving an estimation of the reduction in tire-wear that can be obtained.

5.2 Methodology

The main concept that is used to evaluate tire-wear due to scrubbing deals with the energy loss which is transformed into heat. Due to the generation of this heat, the molecular structure of rubber changes at the contact patch inducing tire wear [11]. The tyre generates heat during its operation mainly during 2 scenarios, these are:

- Due to Lateral Slip.
  The instantaneous power in the lateral direction of the tyre that causes tire-wear due to abrasion is:
  $$P_{sy} = F_y \cdot V_{sy} \tag{5.1}$$
- Due to Longitudinal Slip.
  The instantaneous power in the longitudinal direction can also be measured as:
  $$P_{sx} = F_x \cdot V_{sx} \tag{5.2}$$

It can be said that the sum of (5.1) and (5.2) will be an indicator for the amount of heat generated at a given instant that leads to the wear of the tyre. This means that for a manoeuvre, given the condition that the other factors that affect wear are constant, the wear of the tyre can be calculated by the following formula.

$$W_{tyre} = \int_{t_{start}}^{t_{end}} K_w \cdot (P_{sx} + P_{sy}) dt \tag{5.3}$$

where K_w is a scaling factor whose value is chosen for a given tyre. Its unit is g/W. t_{start} and t_{end} represent the start and stop time of the time interval for which the measurement is taken.

It can be see that the value chosen for the constant K_w will obviously affect the wear results. Hence, it is important that the value of this constant is chosen such that it produces acceptable values of tire wear. It had been decided that the best way to do this is to create the wear calculation of D. Cebon in the Simscape Multibody environment using the MF-Tyre model and compare the values of wear that can be obtained with the proposed method. Then, the constant can be tuned to get similar values of tire-wear.

Choosing the scaling factor K_w

The model used to compare the wear calculations can be seen in Figure 5.1.

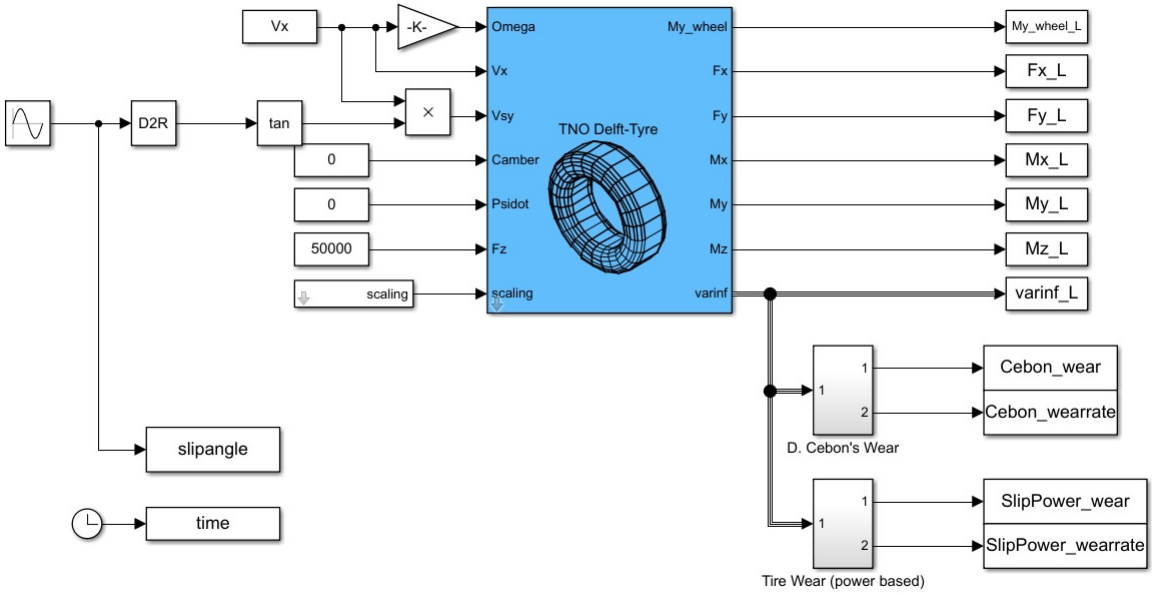

Figure 5.1: Tire Wear Model

The work of D. Cebon [5] calculates tire wear using (2.9). This equation can also be rewritten as:

$$\Delta M = K_1 \int_{t_{start}}^{t_{end}} \alpha^2 \cdot V_x \cdot dt \tag{5.4}$$

where $K_1 = K.w$. Here, $K = 145$ g/m^2 and w is the width of the tyre. t_{start} and t_{end} represent the start and stop time of the time interval for which the measurement is taken.

The normal load on the tyre is maintained at 50 kN as the work of D. Cebon mentions the use of 100 kN load per axle. Since the slip angle is alternated in steps from 0° - 14° in [5], the slip angle input is a sine wave of amplitude 14° and a frequency of 0.05 Hz in the model to assess wear. The work of D. Cebon conducts the experiment at low speeds of 1 - 2 m/s. Testing is conducted at both low speeds (1.4 m/s) and high speeds (14 m/s) to find the

dependency of wear on speed. After obtaining the wear values, it can be seen that similarity in wear values are observed when the constant is chosen as $K_w = 0.0003$ g/W.

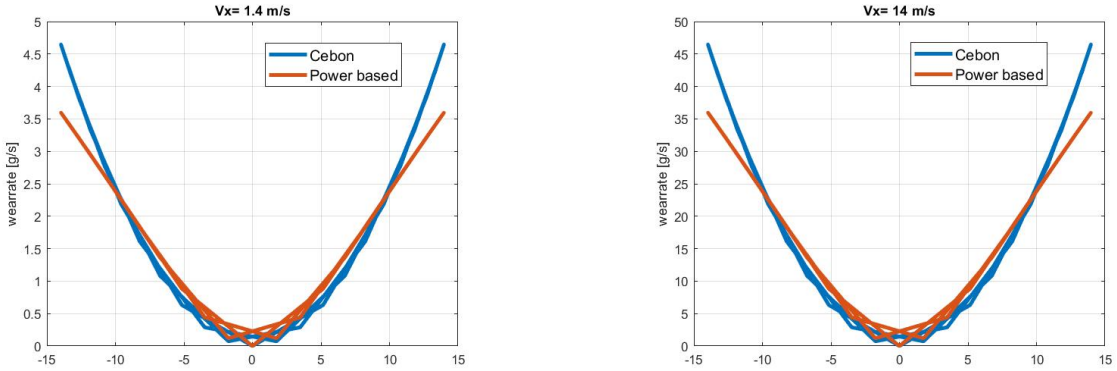

(a) $V_x = 1.4\ m/s^2$ (b) $V_x = 14\ m/s^2$

Figure 5.2: Wear rate for Sine wave input of Slip Angle

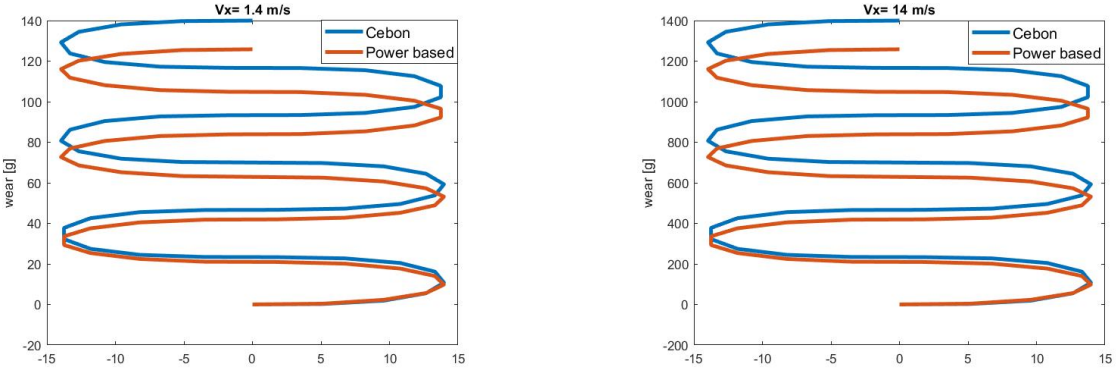

(a) $V_x = 1.4\ m/s^2$ (b) $V_x = 14\ m/s^2$

Figure 5.3: Wear for Sine wave input of Slip Angle

A value of K_1 is chosen that is slightly lower than the value predicted by the calculation of Cebon. In an email correspondence with the author, it had been made clear that the constant K that had been obtained from their experiment is unrealistically large. This is due to the fact that the asphalt used in their testing is rougher than the average roads in the EU. It can be seen in Figure 5.3 that when slip angles are small, the results produced by the proposed formula (5.3) and (5.4) are nearly identical irrespective of the speed of the tyre.

5.3 Comparison of Tire Wear performance

The testing to evaluate the performance gains in terms of tire-wear for the compared tractor semi-trailers is conducted using the following criteria. Both the models of the tractor semitrailer

are made to turn at 90°, 180° and 360°. The speed of the tractor is kept at 7.5 km/h and the radius of the turn is 12.5 m (of that of the EU Circle). The reduction in the magnitude of lateral forces generated at the trailer axles for the 4 axle tractor semi-trailer with trailer axle steering will result in less tire wear. This can be seen in the results for the 360° turn presented in Table 5.1 and 5.2. The complete set of results are presented in Appendix C.

360 ° turn		
Axle	Wear Left tyres [g]	Wear Right tyres [g]
Steer Axle	0.14	0.14
Drive Axle	5.26 — 1.31	1.36 — 5.28
Trailer Axle 1	79.47	42.39
Trailer Axle 2	1.21	0.83
Trailer Axle 3	36.27	52.74
Total Wear	226.4 g	

Table 5.1: Wear during a single 360° turn - 5 axle Tractor Semitrailer

360 ° turn		
Axle	Wear Left tyres [g]	Wear Right tyres [g]
Steer Axle	0.11	0.04
Drive Axle	2.59 — 2.09	1.88 — 2.37
Trailer Axle 1	0.16	0.18
Trailer Axle 2	0.15	0.12
Total Wear	9.69 g	

Table 5.2: Wear during a single 360° turn - 4 axle Tractor Semitrailer with rear axle steering

From the results for the EU 360° turn, we see that the conventional 5 axle tractor semitrailer induces tire-wear that is much higher than the proposed 4 axle tractor semitrailer with rear steering. The wear of the 5 axle combination is $\approx$ 23 times that of the 4 axle tractor semitrailer during one full turn of the EU Circle. Even though the method used to evaluate tire-wear is based on many assumptions, there is still a major reduction seen when using the proposed 4 axle tractor semitrailer. This can be seen from the Figure 5.4. Figure 4.5 shows the single track free body diagrams of the compared vehicle combinations, where the difference in the slip angles generated can be seen. It can be observed from the plot of slip angles during the EU 360° turn (Figure 6.4) that the slip angles generated by the 2 axle semi-trailer are negligible when the rear axle is steered compared to the 3 axle semi-trailer.

It is interesting to note that for the 5 axle combination, severe wear occurs in the front left and rear right tyres of the 3 axle semi-trailer. Trailer axle 1 and trailer axle 3 are further away from the position of the equivalent axle of the 3 axle trailer (Trailer Axle 2). During a low speed turn, the slip angles of the axles that are in front of the equivalent axle are towards the radius of the turn and the slip angles for the axles behind the steering point are away from the radius of the turn as shown in Figure 5.4. Between the left and right tires of Trailer axle 1, the left tyre is towards the inside of the turn and hence would produce greater slip angle due to its smaller turning radius. Similarly, for the tires of Trailer axle 3, the right tire is towards the outside of the turn. Since the direction of generation of slip angles are opposite on the

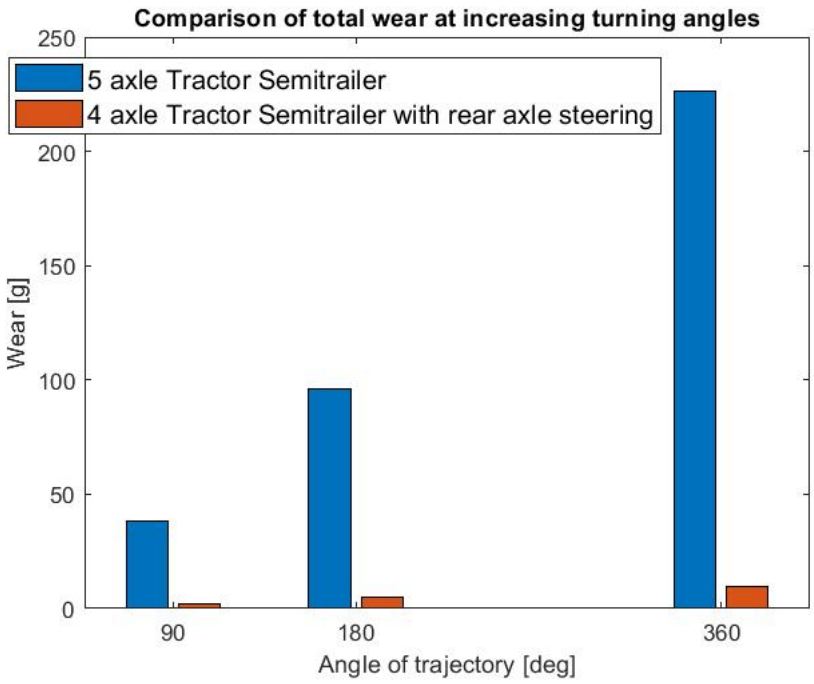

Figure 5.4: Total Vehicle tire-wear during 90°, 180° and 360° turns for both tractor semitrailers

other side of the steering point (Trailer axle 2), the velocity vector of the tyre on the left side is further towards the outside of the turn than the right tyre. However, another reason that influences the trend seen in the generation of tire-wear is the load transfer when turning tight corners. The difference in F_z between the left and right tyres affects the cornering stiffness of each tyre, producing different lateral forces F_y, for the same slip angle. Thus, the product of the normal load F_z shown in Table 5.4 and the slip angle α shown in Table 5.3 gives an indication of the trends for wear shown in Table 5.1 during a left turn of the EU 360° circle.

Axle	**Slip Angle** [°]	
	Left tyre	**Right tyre**
Trailer Axle 1	14.0	10.4
Trailer Axle 2	1.0	0.7
Trailer Axle 3	12.0	8.8

Table 5.3: Slip angles during a left turn of EU 360° circle

Axle	**Normal Load F_z [N]**	
	Left tyre	**Right tyre**
Trailer Axle 1	46200	25500
Trailer Axle 2	36500	34800
Trailer Axle 3	24300	46600

Table 5.4: Normal Load F_z during a left turn of EU 360° circle

5.4 Summary

The chapter begins with a description of the ideas that led to a proposed method to evaluate tire wear. Several methods of tire wear calculation are explored in literature to find one that is best suited to the needs of this thesis. Since tire wear is a complex phenomena and is dependent on many environmental and situational factors, the decision is made to utilize methods that used variables that are available from the tire model and to assume the other factors of influence to be constant. The proposed formula for tire wear is based on empirical estimation of wear proportional to the total energy lost at the contact patch and is meant to be a first estimate to numerically quantify the difference in performance that can be obtained. The results show that the introduction of the rear steered axle will lead to much lower slip forces on the trailer axles of the vehicle, which leads to a significant reduction of tire wear. Although the proposed formula does not predict the exact amount of tire wear, it can be said that one can expect large improvements in the longevity of the trailer tyres when using the 4 axle tractor semitrailer combination with a rear steered axle.

Chapter 6

Comparison by Performance Based Standards

In this chapter the performance of the 2 axle tractor semi-trailer in comparison to the standard tractor semi-trailer is evaluated in terms of manoeuvrability and high speed stability. Three vehicles will be analysed here. The standard Tractor semi-trailer will act as a baseline representing the performance expected from a regular tractor semi-trailer used in the EU. This will be compared to the Tractor semi-trailer with two non steered axles and the tractor semi-trailer with the rear axle being steered via command steering. Performance Based Standards explained in Chapter 2 will be used.

6.1 PBS Results

The performance measures are obtained through simulating the required manoeuvre for each model using the Simscape Multibody version of the TU/e CVL. The dimensions of the trailers that are tested are shared by Knapen Trailers and can be viewed in Figure 3.9.

The semi-trailers are tested at the fully loaded condition as it is the worst case scenario for all procedures, due to the increased center of gravity height and higher load on the tires, which results in larger slip forces.

6.2 Low Speed Tests

In this section, the low speed PBS Tests are evaluated for the Tractor Semi-trailer with 4 axles, with rear steering active & inactive and compared to the baseline Tractor Semi-trailer combination. It can be seen from the Figure 6.1 that the Tractor Semi-trailer of 4 axles without rear steering performs worse than the standard Tractor semi-trailer in its swept path performance. The Tractor Semi-trailer of 4 axles with rear steering has better swept path performance in the EU 360° turn maneuver compared to the 4 axle Tractor Semi-trailer without rear axle steering. The swept path is equal to that of the standard 5 axle Tractor Semi-trailer as seen in Figure 6.3. The cause for these differences will be explained in the next section. The reader can look at the dimensions in Figure 3.9 for reference.

6.2.1 Swept Path

The first PBS Scenario that will be evaluated is the Low speed swept path performance during the EU 360° turn. The swept path performance of the 2 axle semi-trailer without rear axle steering compared to the 3 axle semi-trailer can be seen in Figure 6.1

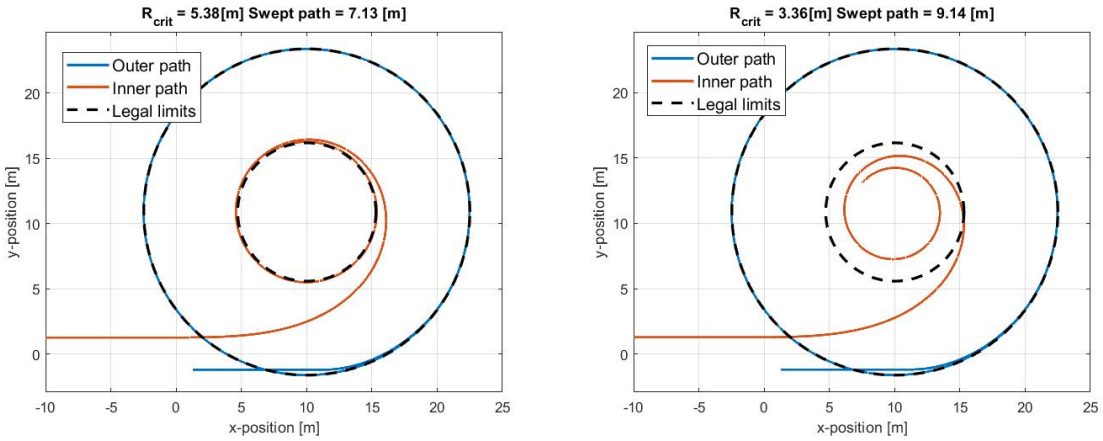

(a) 5 axle Tractor semi-trailer

(b) 4 axle Tractor semi-trailer without rear steering

Figure 6.1: Swept Path - 5 axle vs 4 axle without rear steering

The main contributing factor that affects the swept path performance of a Tractor Semi-trailer combination is the effective wheelbase. The effective wheelbase is defined as the distance from the connection point (fifth wheel) of the trailer to the virtual wheel axle. A straight line drawn along the virtual wheel axle intersects the instantaneous center of the turn the semi-trailer takes. It can be seen as a single axle which represents the axle group as a whole.

For the semi-trailer with 2 axles, this virtual wheel axle is exactly in between the 2 semi-trailer axles, the effective wheelbase is 8.8 m from the 5^{th} wheel. For the semi-trailer with 3 axles, the virtual wheel axle is the middle axle of the tri axle group, making the effective wheelbase 7.75 m from the 5^{th} wheel. Thus the tractor semi-trailer with 3 axles has a shorter effective wheelbase than the tractor semi-trailer with 2 axles. When the trailer moves along a circular path, a shorter effective wheelbase means that the trailer will be closer to the outer radius of the turn, as the effective axle that represents the axle group is now closer to the 5^{th} wheel which increases trailer manoeuvrability. The effective wheelbase of the tractor semi-trailer with 4 axles is too high for it to clear the critical radius condition of $R_{inner} = 5.3$ m set by the EU 360° turn.

Next, the swept path performance of the Tractor semi-trailer with rear steering is explained. Figure 6.3 shows the improvement in the swept path when using the 2 axle semi-trailer with rear axle steering compared to the 3 axle semi-trailer. The improvement in the swept path of the 2 axle semi-trailer with rear steering comes from reducing the effective wheelbase from in between the two axles to the front axle of the semi-trailer for sharp turns. This causes the wheelbase to become 7.7 m from the 5^{th} wheel, which is 0.05 m smaller than the tractor semi-trailer with 3 axles. The inclusion of a steered axle also has the benefit of

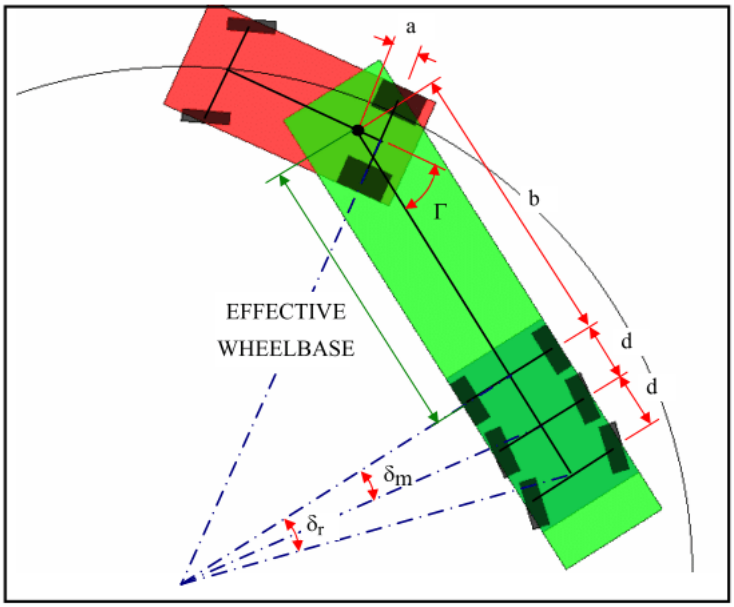

Figure 6.2: Effective Wheelbase [12]

negating the slip angles that are generated at axles which are at a distance from the effective axle. Since the axles in the standard trailer do not have a steering input, the generation of slip angles on the first and third axle produce lateral forces. These forces generate moments that oppose the turning moment of the trailer (induced by the forces at the 5^{th} wheel coupling) causing the resultant force from the equivalent axle (middle axle for the 3 axle semi-trailer) to be reduced. This moves the trailer further towards the inside of the turn. By design, the steered 2 axle trailer eliminates this issue. The slip angles produced during a single EU 360° turn for the 3 axle semi-trailer and the 2 axle semi-trailer with rear axle steering can be observed by referring to Figure 6.4. Hence, the 2 axle semi-trailer is able to have better swept path performance.

6.2.2 Tail Swing

The tail swing of a tractor semi-trailer is dependent on the rear overhang of the semi-trailer. It is measured from the virtual wheel axle to the end of the trailer. The smaller the rear overhang, better the tail swing performance.

The tail swing performance of the 3 combinations compared are now presented. Loading conditions do not affect the tail swing performance significantly, so only the results in the fully loaded condition are shown.

The rear overhang of the standard trailer is 4250 mm while that of the 2 axle trailer without rear steering is 3200 mm. This is due to the effective axle being exactly between the 2 axles. Since the overhang is approximately 25% smaller, the tail swing of the semi-trailer with 2 axles is much smaller. The difference in rear overhang between the 3 axle trailer and the 2 axle trailer with rear axle steering is just 50 mm, as the effective axle is

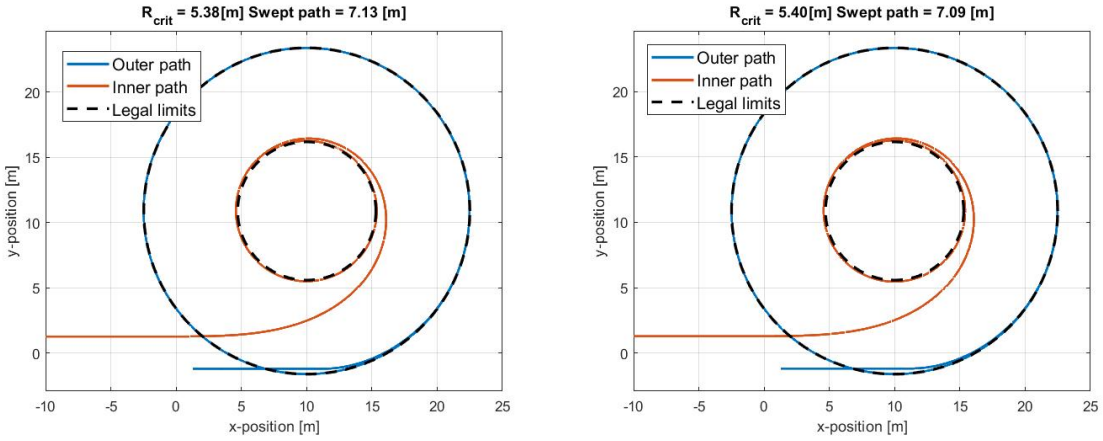

(a) 5 axle Tractor Semi-trailer

(b) 4 axle Tractor Semi-trailer with Command steer rear steering

Figure 6.3: Swept Path - 5 axle vs 4 axle with rear steering

Vehicle Type	**Tail Swing [m]**
5 axle Tractor semi-trailer	0.269
4 axle Tractor semi-trailer — No rear steering	0.108
4 axle Tractor semi-trailer — Rear steering	0.275

Table 6.1: Tail Swing of semi-trailers

now at the position of the first axle of the 2 axle trailer. This small difference means that the tail swing is very similar to that of the conventional tractor semi-trailer, being slightly worse by 2.2%. In conclusion, the swept path of the 2 axle trailer can be greatly improved by introducing rear axle steering while making the tail swing performance only slightly worse than the conventional tractor semi-trailer.

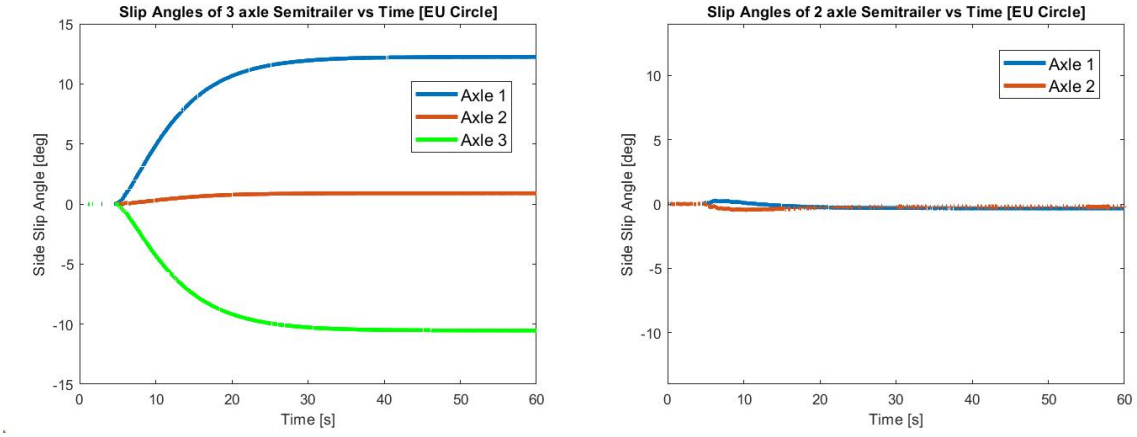

(a) 5 axle Tractor Semi-trailer

(b) 4 axle Tractor Semi-trailer with Command steered rear axle steering

Figure 6.4: Slip angle during EU 360° circle

6.3 High Speed Tests

At high velocities, the yaw damping contributes significantly to the stability of the vehicle. The trailer design parameters can be studied on their contribution to yaw damping by looking at a simplified single track model of a semi-trailer, as stated in [38].

The assumptions here are that the articulation angle and slip angles of the trailer tires are small. Also, for simplicity, the effects of body roll and aerodynamics are neglected and that there is no acceleration of the hauling unit in the longitudinal direction. A simplified free-body diagram of a semi-trailer is shown in Figure 6.5. The tractor attached to the semi-trailer moves in the longitudinal direction with a constant velocity u, with the articulation angle θ being the only degree of freedom.

Here, a represents the distance of the COG of the trailer from the 5^{th} wheel coupling and b represents the distance of the COG of the trailer to the equivalent axle of the axle group. m is the mass of the trailer and $F_{y,t}$ is the lateral force from the 5^{th} wheel. The equation of motion of the trailer is expressed as:

$$(I_{zz} + m(a^2))\ddot{\theta} = (a+b)F_{y,t} \tag{6.1}$$

It is known that,

$$F_{y,t} = C_{f,\alpha} \cdot \alpha_t \tag{6.2}$$

where $C_{f,\alpha}$ is the equivalent cornering stiffness of all the tyres of the axle group and α_t is the equivalent slip angle of the axle group.

Also for small articulation angles ($\theta \approx 0$), the slip angle of the equivalent tyre that represents the axle group α_t can be expressed as:

$$\alpha_t = -(\frac{(a+b)\dot{\theta}}{u} + \theta) \tag{6.3}$$

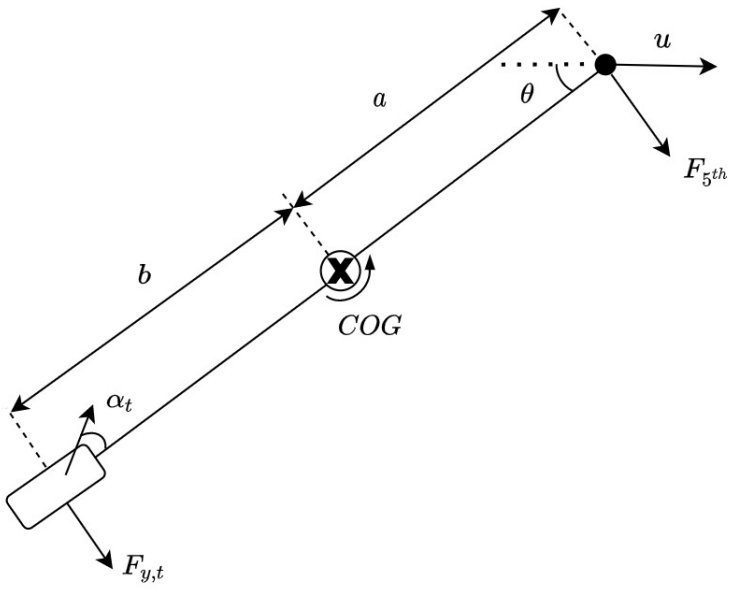

Figure 6.5: Single Track Model

Substituting (6.3) in (6.1) and simplifying, we get:

$$(I_{zz} + m(a^2))\ddot{\theta} + \frac{(a+b)^2}{u} C_{f,\alpha}\dot{\theta} + (a+b)C_{f,\alpha}\theta = 0 \tag{6.4}$$

Equation (6.4) is similar in form to the dynamics of a spring mass damper system. This means that the dimensionless damping coefficient of articulation angle can be formulated according to the formula for the damping coefficient of the spring mass damper system.

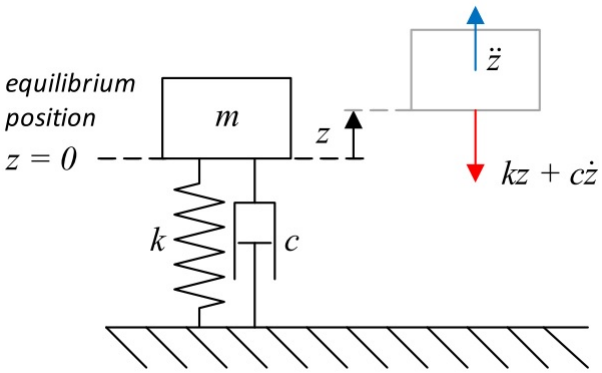

Figure 6.6: Mass-Spring Damper System [13]

If the dynamics of a mass-spring damper system shown in Figure 6.6 are of the form:

$$m\ddot{z} + c\dot{z} + kz = 0 \tag{6.5}$$

where z is the displacement, m is the mass, c is the damping constant and k is the spring

constant.

The dimensionless damping coefficient of the system τ is $\tau = \frac{c}{2\sqrt{mk}}$.

This means that the damping coefficient of the articulation angle of the trailer system τ_θ can be formulated from (6.4) as:

$$\tau_\theta = \frac{(a+b)^2 C_{f\alpha}}{2u\sqrt{(I_{zz}+ma^2)(a+b)C_{f\alpha}}} \tag{6.6}$$

or

$$\tau_\theta = \frac{(a+b)^{1.5} C_{f\alpha}^{0.5}}{2u\sqrt{(I_{zz}+ma^2)}} \tag{6.7}$$

From the equation for damping of the articulation angle (6.7), it follows that:

- Increasing the velocity u of the trailing unit is inversely proportional to the damping of the articulation angle.
- Damping of the articulation angle is proportional to the power of 1.5 of the effective wheelbase $(a+b)$.
- Damping of the articulation angle is inversely proportional to the square-root of the mass of the trailer m.
- Damping of the articulation angle is directly proportional to the square-root of the cornering stiffness $C_{f\alpha}$.

6.3.1 Static Rollover Threshold

Since the gross vehicle weight and COG height of the tractor semi-trailer combinations compared are the same, one can expect that the static rollover thresholds are within the same range. It is to be noted here that since the EU does not use the PBS Standards, we use the values recommended by the Australian Road Transport Suppliers Association (ARTSA) as a baseline of comparison. It is a necessity that the SRT value must be above 0.35 g, which is what is recommended by ARTSA. [6]

The tractor semi-trailer with 3 axles has an SRT value of 0.37 g, which is considered acceptable for a vehicle that is not used to transport hazardous goods and people. For buses and tankers that do carry goods that need more care, a higher rollover threshold of 0.4 g is recommended.

The tractor semi-trailer with 2 axles is found to have a slightly lower SRT of 0.36 g for both command steered and locked wheels. The effect of rear axle steering is almost non-existent when the radius of the turn is 100 m.

It can be seen that all 3 vehicles compared actually do perform very similarly with respect to the static rollover threshold as expected. In general, for vehicles of a similar type, having the same number of articulations and same type of coupling and of the same gross vehicle weight, static rollover thresholds will be close to one another.

6.3.2 High Speed Transient Off-tracking and Rearward Amplification

The high speed off-tracking performance is related to the damping of the articulation angle. Compared to the 3 axle semi-trailer whose effective wheelbase is at a distance of 7750 mm from the 5th wheel, the 2 axle semi-trailer without rear steering will have better off-tracking performance due to its effective wheelbase being 8800 mm from the 5th wheel.

When the single sine procedure is conducted, the lateral acceleration achieved at the steer axle should be a minimum of 0.15g. This will produce a lateral displacement of about 2.5 -3.5 m depending on which tractor semi-trailer is used. It is observed that the overshoot distance of the tractor semi-trailer with 3 axles is 0.251 m. The ARTSA recommends that an overshoot distance of 0.6 m is the maximum allowed. The 3 axle trailer complies with this as it has an overshoot distance of 0.25 as seen in Table 6.2. The Tractor semi-trailers with 2 axles had been expected to show better performance due to the longer effective wheelbase, and that the command steered trailer would be worse off in performance due to the command steering reducing the effective wheelbase. The results show however that the overshoot distance remains the same for both Tractor semi-trailers.

Vehicle Type	**Overshoot Distance [m]**
5 axle Tractor semi-trailer	0.25
4 axle Tractor semi-trailer — No rear steering	0.09
4 axle Tractor semi-trailer — Rear steering	0.09

Table 6.2: Overshoot Distance of Tractor semi-trailers

Command steering is only dependent on the articulation angle of the trailers. To explain the lack of difference in overshoot distance between the 2 axle semi-trailers, we need to look at the variation of a set of parameters that affect trailer behavior. These are:

- Articulation Angle
- Slip forces and slip angles generated
- Angles obtained at rear axles due to rear steering

From the Figure 6.8, it can be seen that the articulation angles of the 2 axle semi-trailers are much better damped than the 3 axle semi-trailer. This highlights the difference in effective wheelbase distances between the 2 axle and 3 axle trailers. We know that the parameters that affect damping of trailer articulation angles are the effective wheelbase, cornering stiffness, longitudinal velocity and mass of trailer.

To study the instability caused by command steering, the Single Sine maneuver was done with increasing amplitude to produce lateral acceleration at the steer axle that is 1.5 times, 2 times and more than 2 times the 0.15 g specified by the ISO Standard. The results of overshoot distances produced are listed in Table 6.3.

When the lateral acceleration at the steer axle is higher, a greater articulation angle is induced, producing more steering input at the rear axle as shown in Figure 6.9. This worsens

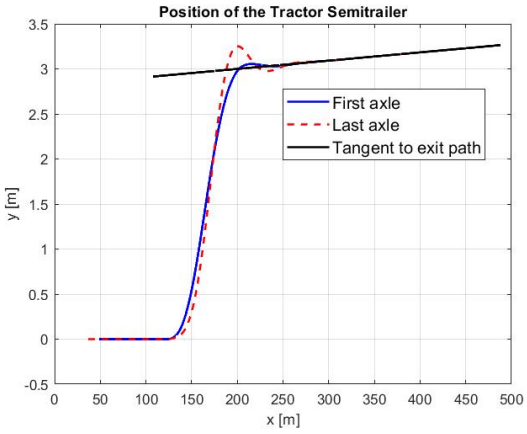

(a) 5 axle Tractor semi-trailer

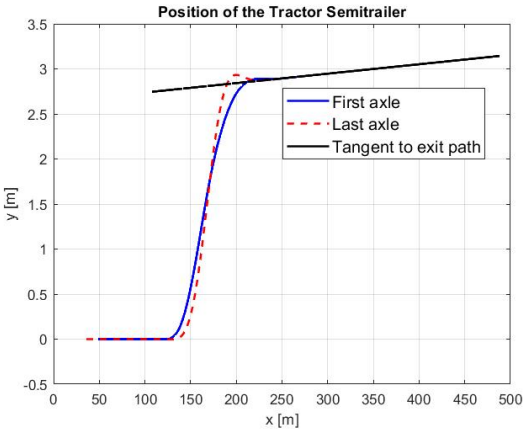

(b) 4 axle Tractor semi-trailer (CS)

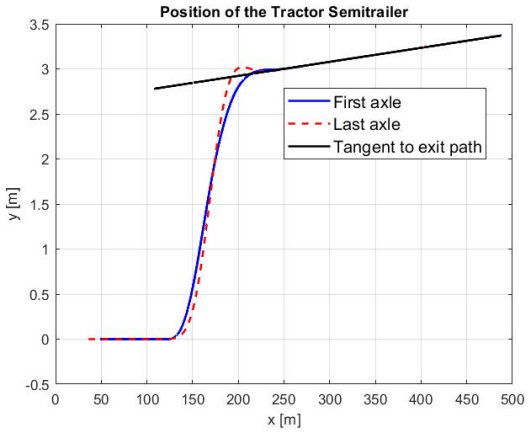

(c) 4 axle Tractor semi-trailer (Locked)

Figure 6.7: Overshoot Distances of Tractor semi-trailers

the effects mentioned earlier, and reduces the stability of the 2 axle trailer even further. We can see a greater disparity in the overshoot distances between the 2 axle semi-trailers, when the lateral acceleration is increased. The 2 axle semi-trailer with locked rear axle is more stable at high lateral accelerations. Note that the command steered 2 axle semi-trailer still fares better than the conventional 3 axle tractor semi-trailer, with the difference becoming smaller at higher lateral accelerations.

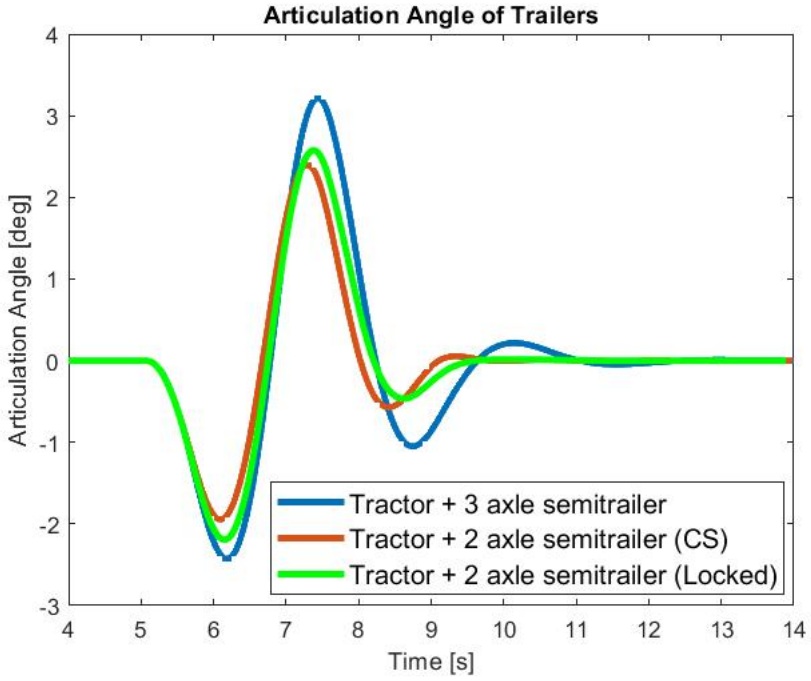

Figure 6.8: Articulation angles of tractor semi-trailers during single sine lane change

Vehicle Type	**0.15 g**	**0.225 g**	**0.3 g**	**0.34 g**
5 axle Tractor semi-trailer	0.25	0.44	0.75	0.85
4 axle Tractor semi-trailer — Rear Steering	0.09	0.19	0.43	0.58
4 axle Tractor semi-trailer — No rear steering	0.09	0.17	0.34	0.44

Table 6.3: Overshoot distance with sine wave input of increasing $a_{y,steer-axle}$

To study the impact of the self-steered axle on the overshoot distance in comparison to an equivalent trailer without a self-steered axle, two conditions of operation are studied. The 2 axle semi-trailer undergoes the single sine lane change for the following conditions:

1. Condition 1: The cornering stiffness of the semi-trailer rear axle is set to 0. This setup mimics how the trailer would operate if the rear axle is a self-steering axle.

2. Condition 2: The cornering stiffness of the tire on both trailer axles in the 2 axle semi-trailer are made to 50% of the total cornering stiffness available. This setup is used to represent the case where the trailer has an equivalent cornering stiffness to that of the self steered case, but has non-steered axles (and hence mimics a trailer with command steered rear axle as negligible steering angles are induced during the single sine lane change manoeuvre).

The overshoot distances are calculated and are listed in Table 6.4:

The overshoot distance of Condition 2 is less than half that of condition 1, even though they have the same overall cornering stiffness. This can be explained by looking at the formula for damping of articulation angle (6.7).

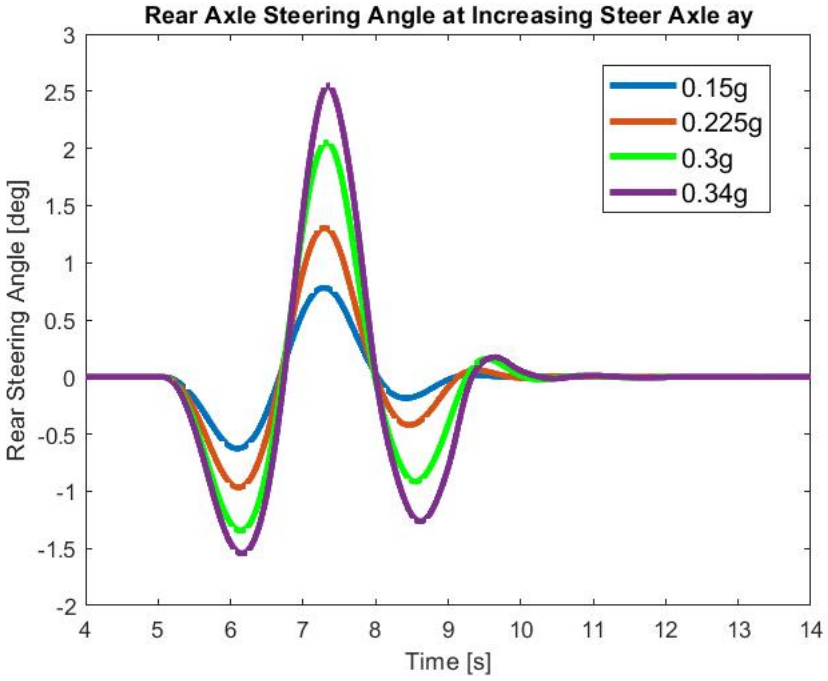

Figure 6.9: Rear axle steering angle at increasing a_y of Single Sine lane change

Scenario	**Overshoot Distance [m]**
Condition 1	1.06
Condition 2	0.44

Table 6.4: Overshoot distance of tested conditions

The overshoot distance depends on $(a+b)^{1.5}$ which is the distance of the 5^{th} wheel coupling from the effective wheel axle. Even though the cornering stiffness is the same, the location of the effective axle is still almost 1 m further away from the 5^{th} wheel than the semi-trailer simulated using Condition 1. This increases the damping coefficient significantly, resulting in a smaller overshoot distance. However in operation, self steered axles are locked above 40 km/h to increase high speed stability.

Vehicle Type	**Rearward Amplification**
5 axle Tractor semi-trailer	1.63
4 axle Tractor semi-trailer — Rear axle steering	1.13
4 axle Tractor semi-trailer — No rear axle steering	1.09

Table 6.5: Rearward Amplification of Tractor semi-trailers

The rearward amplification of the compared vehicles are listed in Table 6.5. The rearward amplification values also favor the 2 axle semi-trailers for the same reasons mentioned above. The difference in performance between the 2 axle semi-trailers is not high as the lateral acceleration at the steer axle is not large enough to amplify the action of the rear steering. If

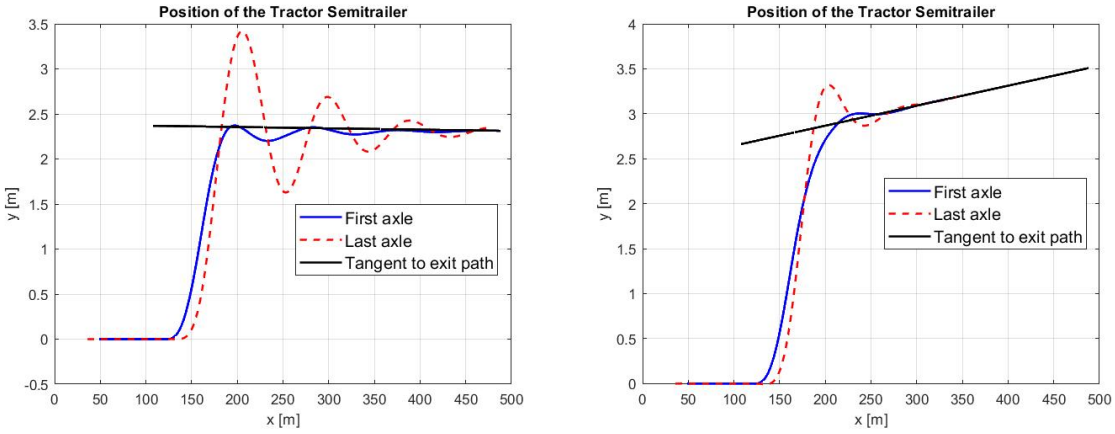

(a) Condition 1

(b) Condition 2

Figure 6.10: Trajectory of 4 axle tractor semi-trailer subject to both conditions

the Single Sine lane change is conducted at greater values of lateral acceleration, the negative effects of low speed command steering at high speed maneuvers will be more visible.

6.3.3 Yaw Damping

During a pulse input, when the tires of the hauling unit cause a force on the 5^{th} wheel coupling, the trailing unit tries to counteract these forces through the lateral force generated by its tires. This introduces oscillations as the trailer tries to attain equilibrium after a sudden change in direction. The ability of a trailing unit to damp yaw oscillations induced by the lateral force acting at the coupling point is expressed by yaw damping. The damping of the yaw rate experienced at the trailer chassis is proportional to the damping of the articulation angle. This can be observed in the similarity of the yaw rate plot (Figure 6.11) to the articulation angle plot (Figure 6.8). Thus the same trends seen between the compared tractor semi-trailer combinations in the High Speed Off-tracking section can also be expected in Yaw Damping.

From (6.7), it can be seen that the damping of articulation angle and yaw-rate is proportional to the effective wheelbase. The reduction of yaw rate observed between the tractor semi-trailer combinations can be summarized in Figure 6.11. The damping effect can be observed when looking at the second and third peak.

This effect of damping is also seen in the lateral acceleration of the semi-trailer chassis, where the peak of lateral acceleration is highest at the chassis of the 3 axle semi-trailer, followed by the 2 axle semi-trailer with command steering. The lowest lateral acceleration is experienced by the 2 axle tractor semi-trailer without rear axle steering.

Even with command steering active during the single sine lane change at 0.15 g, the 2 axle semi-trailer shows better yaw damping performance than the 3 axle semi-trailer. This is a result of only small steering angles being introduced at the rear axle wheels for the single sine lane change of 0.15 g as can be seen from Figure 6.9. Since the steering angle is almost

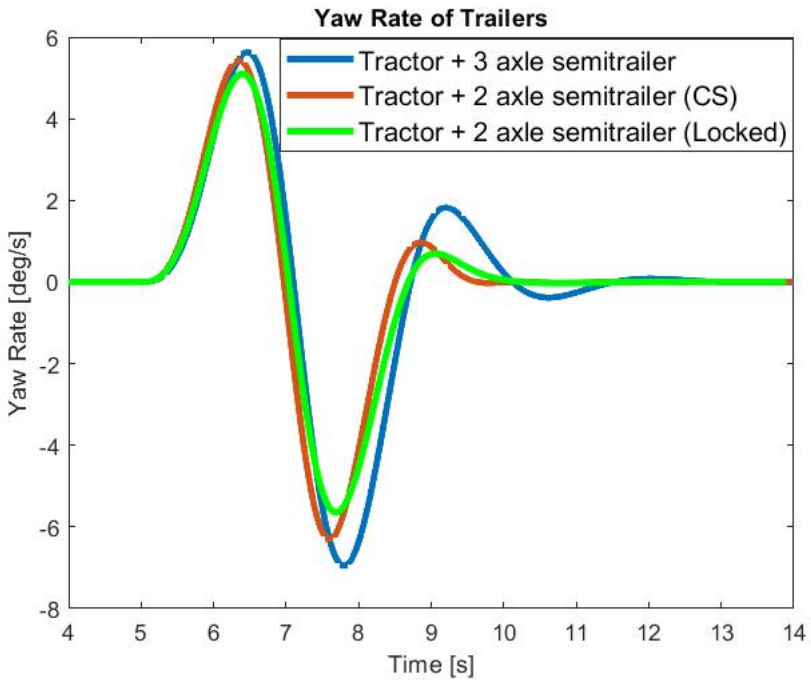

Figure 6.11: Yaw Rate of Tractor semi-trailers

Vehicle Type	**Yaw Damping Ratio**
5 axle Tractor semi-trailer	0.42
4 axle Tractor semi-trailer — Rear steering	0.55
4 axle Tractor semi-trailer — No Rear steering	0.62

Table 6.6: Yaw Damping Ratio of tractor semi-trailers

negligible, the effective wheelbase remains approximately the same as that of the 2 axle semi-trailer with locked rear axle.

6.3.4 Summary

The performance of the 4 axle tractor semi-trailer is compared with the 5 axle tractor semi-trailer using manoeuvres defined in the Australian Performance Based Standards. The results of low speed testing suggest that the introduction of the rear steered axle improves the manoeuvrability of the 4 axle tractor semi-trailer significantly, allowing it to pass the swept path and tail swing criteria for operation in the EU. High speed performance testing shows that the 4 axle tractor semi-trailer with the command steered rear axle has better high speed stability than the 5 axle tractor semi-trailer. The reduction in the distance of the effective wheelbase is not significant for a Single Sine lane change of 0.15 g. At higher lateral accelerations, there is an increase in the rear axle steering angle introduced by command steering. However even at these higher lateral accelerations, the 2 axle semi-trailer with the command steered rear axle has lower overshoot distances than the conventional tractor semi-trailer at the same lateral accelerations. This means that the effective wheelbase of the

4 axle tractor semi-trailer continues to be larger than the wheelbase of the 5 axle tractor semi-trailer even when the command steering is active. A larger effective wheelbase results in greater high speed stability, as can be concluded from the formula for the damping of the articulation angle (6.7). This trend is prevalent in the results of High Speed Off-tracking, Rearward Amplification and Yaw Damping. Overall, there are significant performance gains that can be attained when using the 4 axle tractor semi-trailer with command steered rear axle over the conventional 5 axle tractor semi-trailer. Table 6.7 lists the values obtained for the comparison of trailers using the PBS Standards. The 2 axle trailer with rear axle steering is abbreviated as (RAS) here.

PBS Measure	**Trailer Type**		
Low Speed Manoeuvres	**3 axle**	**2 axle - No RAS**	**2 axle - RAS**
Swept Path	7.13 [m]	9.14 [m]	7.09 [m]
Tail Swing	0.269 [m]	0.108 [m]	0.275 [m]
High Speed Manoeuvres	**3 axle**	**2 axle - No RAS**	**2 axle - RAS**
Static Rollover Threshold	0.37 [g]	0.36 [g]	0.36 [g]
High Speed Off-tracking	0.25 [m]	0.09 [m]	0.09 [m]
Rearward Amplification	1.63	1.09	1.13
Yaw Damping	0.42	0.62	0.55

Table 6.7: List of PBS performance measures and values

Chapter 7

Conclusions and Recommendations

The main focus of this project is on comparing the 4 axle tractor semitrailer with command steered rear axle against a 5 axle tractor semitrailer such that the performance differences between them can be quantified. The section below presents the conclusions from the research and recommendations for a continuation of this work.

7.1 Conclusions

The aim of this thesis is to answer the main research question, which is:

"Will the 2 axle semi-trailer with steered rear axle offer better performance compared to the 3 axle semitrailer to justify its operation in the EU?"

The tractor semitrailers are evaluated in terms of their performance on fuel consumption, tire wear and safety. To make the existing model capable of calculating fuel consumption, an improved power-train model has been developed. With this, the fuel consumption of the vehicle has been evaluated in 2 main scenarios: straight line driving and driving in a circle. The testing of the vehicle has been done for both the 4 axle and 5 axle models of the tractor semitrailer equipped with regional distribution tyres and long haul tyres. The results of both regional and long haul tires show that the difference in fuel consumption continues to decrease as the gross vehicle weight of the vehicle increases. In the fully loaded condition (G.V.W = 40 ton), the difference in fuel consumption is 0.25%. This is a negligible difference, and the reason for this is the small difference in the sum total of rolling resistance force of all tyres combined between the compared tractor semitrailers. Since the 2 axle semitrailer is 1000 kg lighter due to its construction, it carries 1000 kg more payload. When the fuel consumption is calculated on a per ton km basis, we find that the percentage difference between the 2 trailer types is 4.53% for the regional distribution tyres and 4.2% for long haul tyres. There is a significant percentage decrease in fuel consumption per ton.km of payload.

Since the slip forces developed by the 2 axle semitrailer with rear axle steering is much less than that of the 3 axle semitrailer, the lateral 5^{th} wheel forces that the tractor must deal with is also minimized. This means that there is an improvement in the fuel consumption performance when the 2 axle semitrailer conducts a circular turn. This reasoning is reflected in the results as the fuel consumption of the 2 axle semitrailer is almost 66% lower than the

3 axle semitrailer. This means that on top of the gains per ton km of payload, a reduction in absolute fuel consumption is expected when circular turns are involved. Thus depending on how many turns exist in the route taken, there is a potential for considerable gains in terms of fuel consumption when using the 2 axle semitrailer.

The safety performance between the tractor semitrailers are evaluated using manoeuvres mentioned in the Australian Performance Based Standards. The comparison has been done for the 3 axle semitrailer, 2 axle semitrailer with rear axle steering and the 2 axle semitrailer without rear axle steering. The swept path performance of the 2 axle semitrailer with rear axle steering is slightly better that of the 3 axle semitrailer as they share almost the same effective wheelbase due to the action of the rear axle steering, and hence it clears the EU Circle. The 2 axle semitrailer with the locked rear axle has a swept path of 9.14 m, which is more than the swept path of the other trailers and does not clear the EU Circle requirement of 7.25 m. The tail swing performance of the semitrailers depend on the rear overhang (length of trailer - effective wheelbase). The 2 axle semitrailer with its rear axle locked has the least tail swing. Also, the tail swing of the other trailers are within the recommended value (0.6 m) of ARTSA. The Static Rollover Threshold performances are similar at 0.36 g as they share the same gross vehicle weight of 40 ton. There is only a small difference in the effective wheelbase between the 2 axle semitrailers with locked rear axle and that with the command steered rear axle ($\approx 8.8m$) during the single sine steer input from the PBS Standards [6], while that of the 3 axle semitrailer is significantly lesser at 7.75 m. The result of high speed off-tracking and rearward amplification show that the values of the 2 axle semitrailers do not differ by much, while that of the 3 axle semitrailer is significantly higher. Yaw damping also shows that the 2 axle semitrailer has higher damping than the 3 axle semitrailer even when rear axle steering is active. Thus, the 2 axle semitrailer performs as good as the 3 axle semitrailer in low speed manoeuvres and has better high speed stability.

When we consider the results of the comparison of semitrailers overall, the 2 axle semitrailer is the better tractor semitrailer combination for all points of comparison. This thesis recommends the 2 axle semitrailer with rear axle steering for operation in the EU over the current standard, which is the 3 axle semitrailer.

7.2 Recommendations

Even thought the tractor semi-trailer models are made with the intention of being as close as possible to its real life implementation, there are a few areas where the model falls short. Some of these short comings are expressed as recommendations for developing the model in the future. Some thoughts on the continuation of this thesis are also presented later.

- The power-train model consists of a fuel map which is inaccurate at low engine RPM. Updating this fuel map with one that represents the exact tractor engine used in its real life counterpart will enhance the accuracy of the fuel consumption results. The shift-map that allowed the model to shift the gears of the tractor depending on the wheel speed and engine torque has been created using an offline minimization method, which prioritized minimum fuel consumption. This may not represent the actual driver behaviour where he/she shifts the gear depending on the route that he/she takes. Thus to mirror the

behaviour of the driver, the shift-map should be actively changed depending on the road input, in consideration of scenarios that occur during a specific route, hill climbing and descending etc. Another area where the power-train model can be improved is with the implementation of a clutch model, which cuts power to the drive-train when there is a gearshift. This can further improve the accuracy of the fuel consumption results.

- To realize the full potential for reduction in fuel consumption of the 4 axle tractor semi-trailer with rear axle steering, the driver model must be able to follow a specific route between 2 locations in the real world. To do this, the model must be able to comprehend GPS data between the chosen locations and plan and follow the GPS route between these locations. This would give a clear idea for how effective the 4 axle semitrailer with rear steering is in reducing fuel consumption in comparison to the 5 axle tractor semitrailer.

- The work done in this thesis can be expanded towards the comparison of an optimized Super Eco-combi combination that has the tractor unit hauling two 2 axle semi-trailers with rear axle steering against the standard Eco-combi combination that has the tractor unit hauling two 3 axle tractor semi-trailers. The dolly that the second trailer attaches to, can have both steered and powered wheels, as suggested in the works of [18], [39] and [33]. The comparison can be done for fuel consumption in a straight line and circle. The extra payload capacity of the two 2 axle semi-trailer will decrease the per-ton km fuel consumption considerably, while the reduction in fuel consumption while driving in a circle will be great as well. Gains in tire-wear performance and safety performance can also be tested. Finally, the gains in performance across fuel consumption and tire wear can be tested using an optimized driver module that converts GPS data to data which the path following controller can use. GPS coordinates between two locations can be used then that guide the high capacity vehicles in the simulation environment to travel the exact route specified in the GPS coordinates. Thus, the performance gains that the Super Eco-combi with two 2 axle semi-trailers with rear axle steering and a smart dolly can have over the conventional Eco-combi can be gauged in a realistic scenario for the operation of the vehicle.

Bibliography

[1] European Environment Agency, "Greenhouse gas emissions from transport in Europe," pp. 1–7, 2018. [Online]. Available: https://www.eea.europa.eu/data-and-maps/indicators/transport-emissions-of-greenhouse-gases-7/assessment%0Ahttps://www.eea.europa.eu/data-and-maps/indicators/transport-emissions-of-greenhouse-gases-7/assessment%0Ahttps://www.eea.europa.eu/data-and-maps/ind

[2] B. Jujnovich and D. Cebon, "Comparative performance of semi-trailer steering systems," *Proceedings of the 7th International Symposium on Heavy Vehicle Weights and Dimensions*, pp. 195–214, 2002.

[3] Y. Li, S. Zuo, L. Lei, X. Yang, and X. Wu, "Analysis of Impact factors of tire wear," *JVC/Journal of Vibration and Control*, vol. 18, no. 6, pp. 833–840, 5 2012.

[4] I. Besselink, *Vehicle Dynamics- 4AT100 - Lecture notes of TU/e*, 2020.

[5] J. Lepine and D. Cebon, "Empirical Estimation of Heavy Goods Vehicle Tyre Wear." [Online]. Available: https://hvttforum.org/wp-content/uploads/2019/11/Lepine-EMPIRICAL-ESTIMATION-OF-HEAVY-GOODS-VEHICLE-TYRE-WEAR.pdf

[6] "Performance-Based Standards Scheme – The Standards and Vehicle Assessment Rules," 2020. [Online]. Available: https://www.nhvr.gov.au/files/0020-pbsstdsvehassrules.pdf

[7] ISO, "ISO14791:2000(E) Road Vehicles - Heavy Commercial Vehicle Combinations and Articulated Buses - Lateral Stability Test Methods," 2002. [Online]. Available: https://www.iso.org/standard/25560.html

[8] Mathworks, "Model a Simple Link." [Online]. Available: https://nl.mathworks.com/help/physmod/sm/gs/model-simple-link.html

[9] G. Isiklar, I. Besselink, and H. Nijmeijer, "Simulation of complex articulated commercial vehicles for different driving manoeuvres," Tech. Rep., 2007. [Online]. Available: http://www.mate.tue.nl/mate/pdfs/8505.pdf

[10] "Ackerman Steering." [Online]. Available: https://www.xarg.org/book/kinematics/ackerman-steering/

[11] Michelin, "The Tyre - Rolling Resistance and Fuel Savings," Tech. Rep. 3, 2010. [Online]. Available: http://www.dimnp.unipi.it/guiggiani-m/Michelin_Tire_Rolling_Resistance.pdf

[12] S. Milani, "Modelling, Simulation and Active Control of Tractor Semitrailer Combinations," 2015. [Online]. Available: https://www.researchgate.net/publication/320101925_MODELING_SIMULATION_AND_ACTIVE_CONTROL_OF_TRACTOR-SEMITRAILER_COMBINATIONS

[13] I. Besselink, *Road Vehicle Dynamics - 4AUB20 - Lecture notes of TU/e*, 2020.

[14] "Council Directive 96/53/EC." [Online]. Available: https://eur-lex.europa.eu/legal-content/EN/TXT/PDF/?uri=CELEX:31996L0053&from=NL

[15] "Knapen Trailers." [Online]. Available: https://www.knapen-trailers.eu/

[16] S. Sankar, S. Sankar, S. Rakheja, and A. Piche, "Directional Dynamics of a Tractor-Semitrailer with Self-and Forced-Steering Axles," Tech. Rep., 1991. [Online]. Available: https://www.jstor.org/stable/44471073

[17] K. Rangavajhula and H. S. Tsao, "Effect of multi-axle steering on off-tracking and dynamic lateral response of articulated tractor-trailer combinations," *International Journal of Heavy Vehicle Systems*, vol. 14, no. 4, pp. 376–401, 2007.

[18] R. Wouters, "Preliminary design of a smart powered dolly for an A-double high capacity vehicle," Tech. Rep., 2016. [Online]. Available: https://research.tue.nl/en/studentTheses/preliminary-design-of-a-smart-powered-dolly-for-an-a-double-high-

[19] P. Hatzidimitris, "Active trailer steering control for longer heavier vehicles — Eindhoven University of Technology research portal," 2015. [Online]. Available: https://research.tue.nl/en/studentTheses/active-trailer-steering-control-for-longer-heavier-vehicles

[20] G. d. C. F. Silva, "Applying Tire Models To Michelin Tires for Wear Estimation," Tech. Rep. [Online]. Available: http://www.repositorio.poli.ufrj.br/monografias/monopoli10029789.pdf

[21] K. Kato and K. Adachi, "Wear Mechanisms. Chapter 7 of Modern Tribology Handbook, Ed. B. Bhushan," 2001.

[22] G. Stachowiak and A. Batchelor, *Engineering Tribology*. Cambridge University Press, 2006.

[23] H. Salminen, "Parametrizing tyre wear using a brush tyre mode," Tech. Rep., 2014. [Online]. Available: https://www.diva-portal.org/smash/get/diva2:802101/FULLTEXT01.pdf

[24] M. Mohammadi and R. Ngeno, "Analysis of tyre wear using the expanded brush tyre model (Dissertation)," 2015. [Online]. Available: http://urn.kb.se/resolve?urn=urn:nbn:se:kth:diva-173725

[25] R. Tamada and M. Shiraishi, "Prediction of uneven tire wear using wear progress simulation," *Tire Science and Technology*, vol. 45, no. 2, pp. 87–100, 2017. [Online]. Available: https://jglobal.jst.go.jp/en/detail?JGLOBAL_ID=202002222871949825

[26] F. Braghin, F. Cheli, S. Melzi, and F. Resta, "Tyre wear model: Validation and sensitivity analysis," *Meccanica*, vol. 41, no. 2, pp. 143–156, 4 2006. [Online]. Available: https://link.springer.com/article/10.1007/s11012-005-1058-9

[27] H. Pacejka, *Tire and vehicle dynamics*. Elsevier, 2005.

[28] I. Besselink, B. Kraaijenhagen, and J. Pauwelussen, "Greening and safety assurance of future modular road vehicles." [Online]. Available: https://research.tue.nl/en/publications/greening-and-safety-assurance-of-future-modular-road-vehicles

[29] MATLAB, "Gaussian curve membership function - MATLAB gaussmf." [Online]. Available: https://www.mathworks.com/help/fuzzy/gaussmf.html

[30] Mathworks, "Simscape Multibody - MATLAB & Simulink," 2021. [Online]. Available: https://www.mathworks.com/products/simscape-multibody.html#imcad%0Ahttps://uk.mathworks.com/products/simmechanics.html?s_eid=PSM_15028

[31] ——, "Working with Frames - Simscape Multibody Documentation." [Online]. Available: https://nl.mathworks.com/help/physmod/sm/ug/frames-and-frame-transforms.html

[32] ——, "Modeling Bodies." [Online]. Available: https://nl.mathworks.com/help/physmod/sm/ug/simmechanics-bodies.html

[33] A. G. P. Parfant, R. Wouters, and I. Besselink, "Design and Analysis of a Powered Dolly Concept for an A-double High Capacity Vehicle," Tech. Rep., 2017. [Online]. Available: https://hvttforum.org/wp-content/uploads/2019/11/Besselink-STEERED-AND-POWERED-DOLLY-FOR-AN-A-DOUBLE-HIGH-CAPACITY-VEHICLE.pdf

[34] DAF Netherlands, "DAF XF Powertrain - DAF Netherlands." [Online]. Available: https://www.daf.nl/nl-nl/trucks/daf-xf/daf-xf-aandrijflijn

[35] ZF, "Truck Driveline - ZF." [Online]. Available: https://www.zf.com/products/en/trucks/productfinder/driveline.html

[36] S. W. Hunt, A. M. Odhams, R. L. Roebuck, and D. Cebon, "Parameter measurement for heavy-vehicle fuel consumption modelling," in *Proceedings of the Institution of Mechanical Engineers, Part D: Journal of Automobile Engineering*, vol. 225, no. 5. SAGE PublicationsSage UK: London, England, 5 2011, pp. 567–589. [Online]. Available: https://journals.sagepub.com/doi/abs/10.1177/2041299110394512

[37] Wikipedia, "Speed limits in the Netherlands - Wikipedia." [Online]. Available: https://en.wikipedia.org/wiki/Speed_limits_in_the_Netherlands

[38] D. Karnopp, *Vehicle dynamics, stability, and control*. CRC Press, 2013.

[39] S. Franz and M. Hofmann, "Real-Time Control Interface for a Steered and Braked Converter Dolly for High Capacity Transport Vehicles," 2015. [Online]. Available: https://odr.chalmers.se/handle/20.500.12380/219326

Appendix A

Fuel Consumption Results

The absolute fuel consumption (L/100km) for the 5 axle and 4 axle tractor semi-trailers are presented in Tables A.1 and A.2.

5 axle Tractor Semi-trailer	**Fuel Consumption [L/100km]**					
	Regional distribution tyres			**Long haul tyres**		
	Payload (ton)			*Payload (ton)*		
Speed (km/h)	**0**	**12.5**	**25**	**0**	**12.5**	**25**
50	16.07	18.85	21.45	15.72	18.17	20.46
60	19.36	22.19	24.83	19	21.5	23.82
70	22.69	25.51	28.13	22.33	24.81	27.12
80	25.53	28.25	30.77	25.17	27.57	29.78

Table A.1: Fuel consumption (L/100km) - 5 axle tractor semi-trailer

4 axle Tractor Semi-trailer	**Fuel Consumption [L/100km]**							
	Regional distribution tyres				**Long haul tyres**			
	Payload (ton)				*Payload (ton)*			
Speed (km/h)	**0**	**12.5**	**25**	**26**	**0**	**12.5**	**25**	**26**
50	15.78	18.57	21.15	21.36	15.47	17.94	20.24	20.42
60	19.07	21.91	24.53	24.74	18.74	21.28	23.6	23.78
70	22.41	25.22	27.83	28.03	22.08	24.58	26.89	27.07
80	25.25	27.97	30.48	30.68	24.93	27.34	29.56	29.73

Table A.2: Fuel consumption (L/100km) - 4 axle tractor semi-trailer

Appendix B

Yaw Damping with increasing distance between axles

In the discussion of yaw damping, it was seen that the critical factor within the dimensions of the trailer that affected yaw damping was the distance of the effective wheelbase. However, another important factor that affects yaw damping performance is the distance of the axles in the axle group from the effective wheel axle. This distance from the effective wheel axle position increases the length of the moment arm (and thereby increases the force) that can counter the yaw moment produced due to the force at the 5^{th} wheel coupling. To test this effect, the distance between axles of the 3 axle semitrailer was incremented 5 cm at a time and subject to the yaw damping manoeuvre. The plot (Figure B.1) shows that the peak yaw-rate decreases while the yaw damping coefficient increases as the distance between the axle groups are increased. However, the decision to increase the distance between the axles for a trailer also comes at a risk of increasing the slip angles the wheels apart from the ones on the effective wheel axle. This can drastically affect the fuel consumption and tire wear of the trailer.

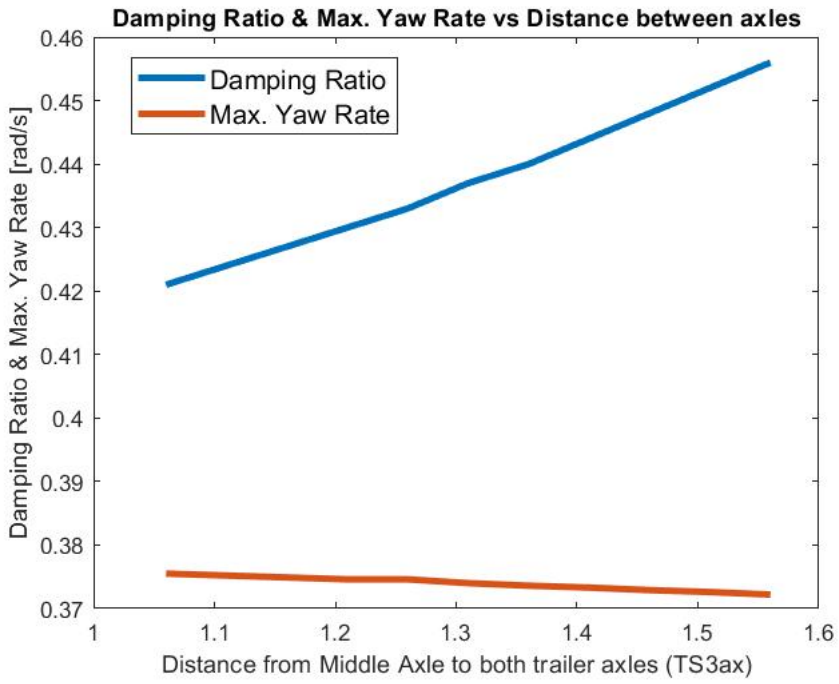

Figure B.1: Yaw Damping and Max. yaw rate vs Distance between axles

Appendix C

Tire Wear Results

The results of tire-wear for the 90°, 180° and 360° turn are presented for the 5 axle Tractor Semi-trailer in Tables C.1,C.2 & C.3 and for the 4 axle Tractor Semi-trailer in Tables C.4, C.5 & C.6.

5 axle Tractor Semi-trailer	**Tire Wear [g]**			
90° turn	**Formulae Used**			
	$W_{tyre} = K_1 \int \alpha^2 \cdot V_x \cdot dt$		$W_{tyre} = \int_{t=t_{start}}^{t=t_{end}} K_w \cdot (P_{sx} + P_{sy}) dt$	
Axle	**Left**	**Right**	**Left**	**Right**
Steer Axle	0.086	0.077	0.14	0.14
Drive Axle	0.094 | 0.092	0.082 | 0.084	0.93 | 0.41	0.43 | 0.94
Trailer Axle 1	7.77	6.8	12.71	7.82
Trailer Axle 2	0.063	0.054	0.11	0.094
Trailer Axle 3	5.26	4.6	6.37	8.11
Total Wear	**25.06**		**38.2**	

Table C.1: Tire Wear TS3ax - 90° turn

5 axle Tractor Semi-trailer	**Tire Wear [g]**			
180° turn	**Formulae Used**			
	$W_{tyre} = K_1 \int \alpha^2 \cdot V_x \cdot dt$		$W_{tyre} = \int_{t=t_{start}}^{t=t_{end}} K_w \cdot (P_{sx} + P_{sy}) dt$	
Axle	**Left**	**Right**	**Left**	**Right**
Steer Axle	0.17	0.16	0.28	0.29
Drive Axle	0.2 | 0.19	0.17 | 0.17	0.93 | 0.41	0.43 | 0.94
Trailer Axle 1	25.3	20.72	34.34	19.14
Trailer Axle 2	0.23	0.19	0.42	0.31
Trailer Axle 3	16.73	13.68	16.1	22.25
Total Wear	**77.75**		**95.84**	

Table C.2: Tire Wear TS3ax - 180° turn

5 axle Tractor Semi-trailer	**Tire Wear [g]**			
360° turn	**Formulae Used**			
	$W_{tyre} = K_1 \int \alpha^2 \cdot V_x \cdot dt$		$W_{tyre} = \int_{t=t_{start}}^{t=t_{end}} K_w \cdot (P_{sx} + P_{sy}) dt$	
Axle	**Left**	**Right**	**Left**	**Right**
Steer Axle	0.35	0.32	0.56	0.56
Drive Axle	0.38 | 0.37	0.32 | 0.32	5.26 | 1.31	1.36 | 5.28
Trailer Axle 1	67.87	53.17	79.47	42.39
Trailer Axle 2	0.66	0.51	1.21	0.83
Trailer Axle 3	44.6	34.8	36.27	52.74
Total Wear	**203.67**		**226.4**	

Table C.3: Tire Wear TS3ax - 360° turn

4 axle Tractor Semi-trailer	**Tire Wear [g]**			
90° turn	**Formulae Used**			
	$W_{tyre} = K_1 \int \alpha^2 \cdot V_x \cdot dt$		$W_{tyre} = \int_{t=t_{start}}^{t=t_{end}} K_w \cdot (P_{sx} + P_{sy}) dt$	
Axle	**Left**	**Right**	**Left**	**Right**
Steer Axle	0.071	0.029	0.11	0.039
Drive Axle	0.0023 | 0.0023	0.002 | 0.002	0.52 | 0.41	0.37 | 0.48
Trailer Axle 1	0.027	0.025	0.093	0.079
Trailer Axle 2	0.025	0.016	0.087	0.061
Total Wear	**0.201**		**2.249**	

Table C.4: Tire Wear TS2ax - 90° turn

4 axle Tractor Semi-trailer	**Tire Wear [g]**			
180° turn	**Formulae Used**			
	$W_{tyre} = K_1 \int \alpha^2 \cdot V_x \cdot dt$		$W_{tyre} = \int_{t=t_{start}}^{t=t_{end}} K_w \cdot (P_{sx} + P_{sy}) dt$	
Axle	**Left**	**Right**	**Left**	**Right**
Steer Axle	0.13	0.034	0.11	0.039
Drive Axle	0.004 | 0.004	0.004 | 0.004	1.24 | 1.00	0.90 | 1.14
Trailer Axle 1	0.046	0.04	0.14	0.14
Trailer Axle 2	0.044	0.023	0.14	0.093
Total Wear	**0.33**		**4.492**	

Table C.5: Tire Wear TS2ax - 180° turn

4 axle Tractor Semi-trailer	**Tire Wear [g]**			
360° turn	**Formulae Used**			
	$W_{tyre} = K_1 \int \alpha^2 \cdot V_x \cdot dt$		$W_{tyre} = \int_{t=t_{start}}^{t=t_{end}} K_w \cdot (P_{sx} + P_{sy}) dt$	
Axle	**Left**	**Right**	**Left**	**Right**
Steer Axle	0.23	0.04	0.11	0.039
Drive Axle	0.0055 | 0.0053	0.0047 | 0.0048	2.59 | 2.09	1.88 | 2.37
Trailer Axle 1	0.059	0.048	0.16	0.18
Trailer Axle 2	0.054	0.028	0.15	0.12
Total Wear	**0.48**		**9.68**	

Table C.6: Tire Wear TS2ax - 360° turn

Appendix D

Derivation of steering angle for rear axle steering

Command steering of the rear axle of the 2 axle tractor semi-trailer depends only on the articulation angle between the tractor and the semi-trailer. To derive the equation for the steering angle, a single track model of the 4 axle tractor semi-trailer with rear axle steering when it is cornering a tight radius turn is shown in Figure D.1

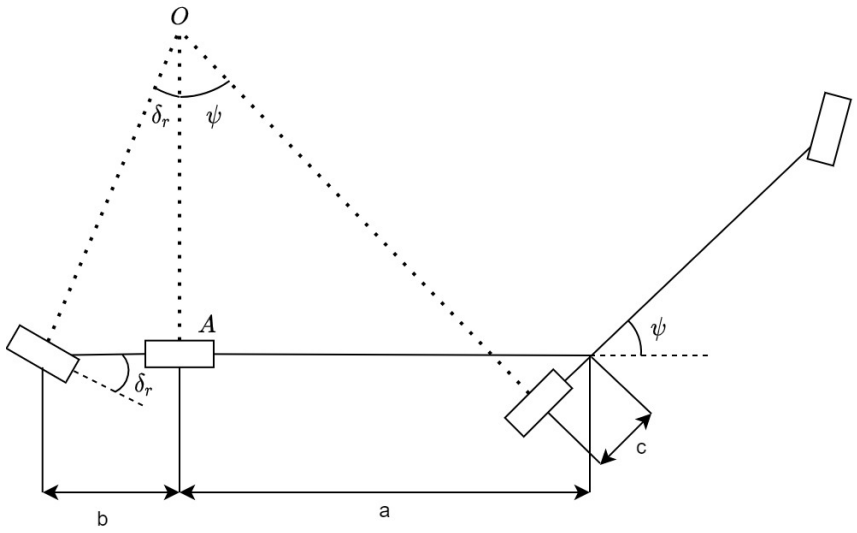

Figure D.1: Single track model of 2 axle semitrailer when cornering

where a is the distance of the 5^{th} wheel to the first axle of the trailer and b is the distance between the first and second axle. The distance c is the distance between the 5^{th} wheel and the drive axle of the tractor. The articulation angle between the tractor and semi-trailer is represented by ψ and the steer angle for the rear axle steering is δ_r. The instant center of cornering is represented by O.

We know that the angle between 2 lines is the same as the angle between the perpendiculars drawn from the lines. This means that the angle between the perpendiculars from the steered rear axle and the non-steered axle is the steer angle δ_r. Also, the angle between the perpendiculars drawn from the non-steered axle and the drive axle of the tractor is the articulation angle ψ.

Now,

$$tan(\psi) = \frac{a - \frac{c}{cos(\psi)}}{OA} \tag{D.1}$$

$$tan(\delta_r) = \frac{b}{OA} \tag{D.2}$$

Eliminating OA from (D.1) and (D.2), we get:

$$\delta_r = arctan(\frac{btan\psi}{a - \frac{c}{cos(\psi)}}) \tag{D.3}$$

Appendix E

Dependency of C_{RR} on normal load Z

To correct the rolling resistance coefficients according to the load acting on each tyre, the dependency of the load on the rolling resistance coefficient is to be known. This equation can be derived as follows.

The effect of vertical force on rolling resistance is defined by:

$$F_{RR} = F_{RR-ISO} \cdot (\frac{Z}{Z_{ISO}})^{\beta} \tag{E.1}$$

Also, we know that the rolling resistance force is defined as:

$$F_{RR} = C_{RR} \cdot Z \tag{E.2}$$

This means that

$$F_{RR_{ISO}} = C_{RR_{ISO}} \cdot Z_{ISO} \tag{E.3}$$

Dividing (E.2) by (E.3), we get:

$$\frac{F_{RR}}{F_{RR_{ISO}}} = \frac{C_{RR}}{C_{RR_{ISO}}} \cdot \frac{Z}{Z_{ISO}} \tag{E.4}$$

Then if we eliminate $\frac{F_{RR}}{F_{RR_{ISO}}}$ by dividing (E.4) with (E.1) and rearrange, we get:

$$C_{RR} = C_{RR-ISO} \cdot (\frac{Z}{Z_{ISO}})^{1-\beta} \tag{E.5}$$

Appendix F

Optimal position of placement of COG for maximum damping coefficient

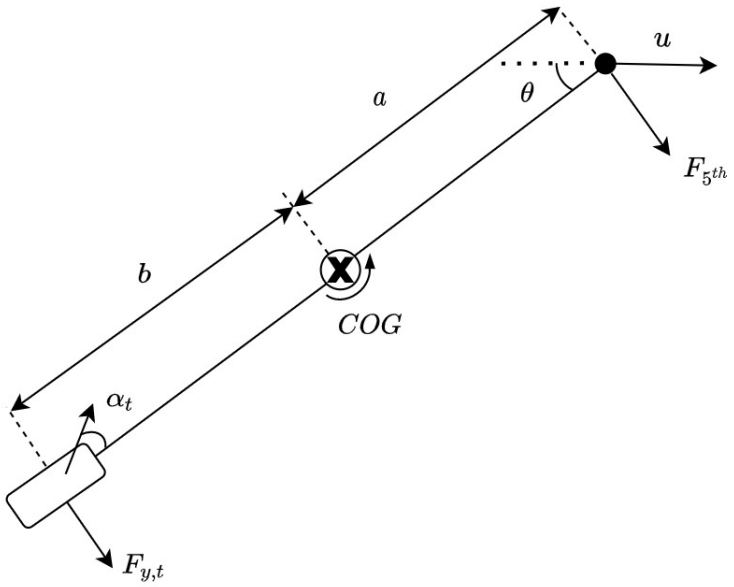

Figure F.1: Single Track Model

The equation for the damping of the articulation angle was derived using Figure F.1 as:

$$\tau_\theta = \frac{(a+b)^{1.5} C_{f\alpha}^{0.5}}{2u\sqrt{(I_{zz} + ma^2)}} \tag{F.1}$$

Differentiating (F.1) with respect to a, we get:

$$\frac{d\tau_\theta}{da} = \frac{2u(I_{zz}+ma^2)^{0.5}\cdot[1.5(a+b)^{0.5}C_{f\alpha}^{0.5}] - (a+b)^{1.5}C_{f\alpha}^{0.5}[2u.0.5.(I_{zz}+ma^2)^{-0.5}2ma}{4u^2(I_{zz}+ma^2)} \tag{F.2}$$

Equating (F.2) to 0 and simplifying, we get:

$$\frac{3}{2}(I_{zz}+ma^2) = (a+b).2ma \tag{F.3}$$

Rearranging, we get the quadratic equation:

$$ma^2 + 4mab - 3I_{zz} = 0 \tag{F.4}$$

The solutions for this equation are:

$$a = -2b \pm \sqrt{4b^2 + \frac{3I_{zz}}{m}} \tag{F.5}$$

Adding b on both sides of (F.5),

$$l = -b \pm \sqrt{4b^2 + \frac{3I_{zz}}{m}} \tag{F.6}$$

It is expected that one of the solutions will be trivial and will not apply to reality.

Using F.6, we can get 2 quadratic equations:

$$3b^2 - 2lb + (-l^2 + \frac{3I_{zz}}{m}) = 0 \tag{F.7}$$

whose solution is

$$b = \frac{l}{3} \pm \sqrt{\frac{8}{3}l^2 - \frac{6I_{zz}}{m}} \tag{F.8}$$

and

$$5b^2 + 2lb + l^2 + \frac{3I_{zz}}{m} = 0 \tag{F.9}$$

whose solution is

$$b = -\frac{l}{5} \pm \sqrt{\frac{-8l^2}{5} - \frac{6I_{zz}}{m}} \tag{F.10}$$

We can see that (F.10) is trivial.

Thus, using (F.8), if the effective wheelbase ($a+b=l$) is known for a vehicle and the total mass of the trailer (m) and the moment of inertia about the z axis (I_{zz}) are known, the COG can be placed at a location that yields maximum damping coefficient, which improves the high speed safety performance of the trailer.

Appendix G

Drive-line Model

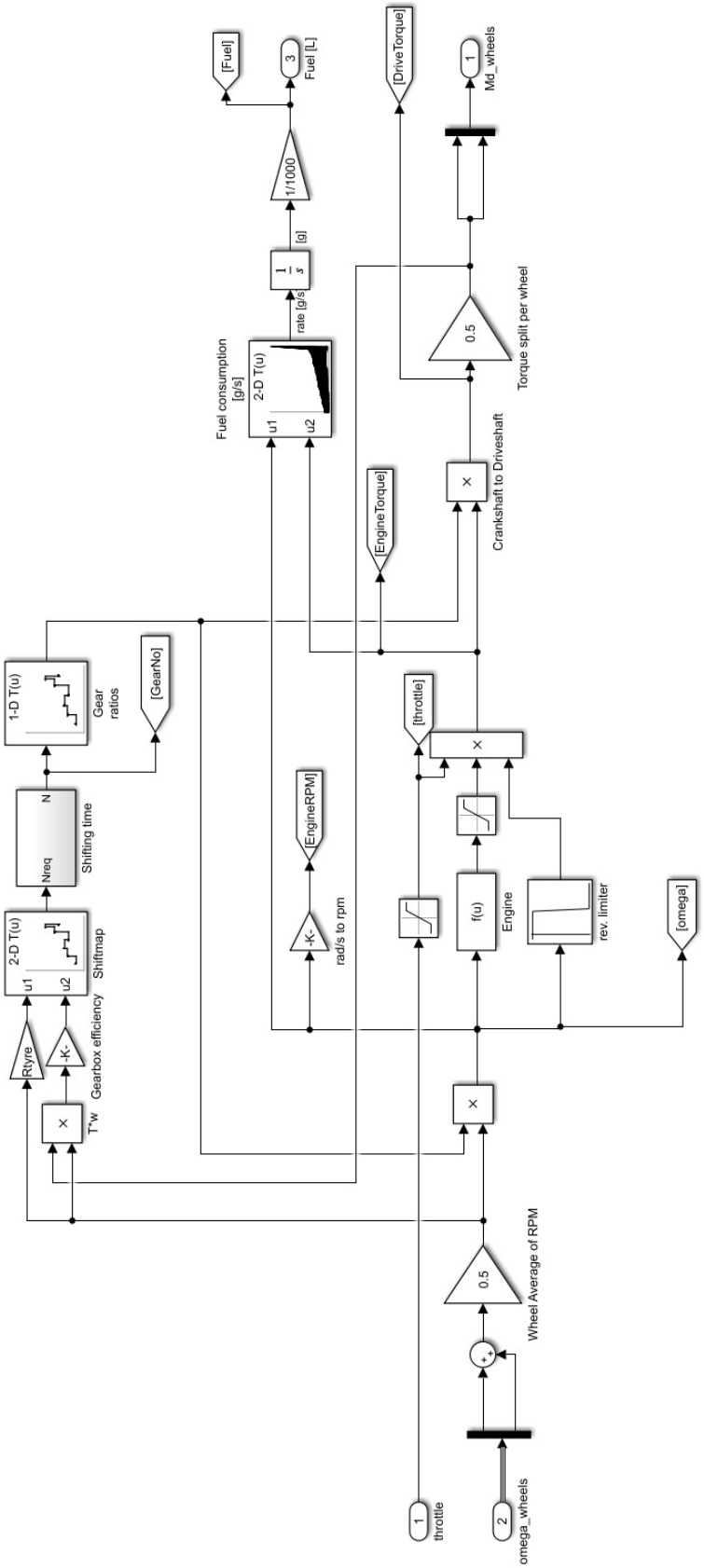

Figure G.1: Drive-line Model